

Faculdade de Engenharia da Universidade do Porto



**Monitoring of the bone consolidation process in  
a tibial fracture**

Renato Pereira de Carvalho

Dissertation submitted for the achievement of the Master Degree in  
Bioengineering

Advisor: Prof. Mário Vaz

Advisor: Dr. Miguel Marta

March 15, 2019



# Resumo

Fraturas na tíbia são das fraturas mais comuns, devido à sua elevada área de superfície. A sua principal função é a provisão de equilíbrio e suporte para o corpo. Fraturas nos ossos longos dos membros inferiores são consideradas complexas e comumente resultam em longos períodos de incapacidade. Após a ocorrência de uma fratura, há muitas propostas para executar a imobilização do osso. Fixadores externos são normalmente utilizados em fraturas “fechadas” e quando o risco de infecção é elevado, conferindo a devida rigidez e estabilidade para o realinhamento do osso fraturado. Os sistemas atuais apenas permitem a análise do progresso da consolidação através do recurso a raios X, o que dificulta a sua avaliação contínua. Além disso, há algumas desvantagens para o paciente, especialmente a sua exposição à radiação, e a dependência na capacidade do operante. Esta tese pretende monitorizar o processo de consolidação óssea através da execução de testes mecânicos de compressão, assim como através da criação de um modelo numérico que simule o seu comportamento e preveja a regeneração óssea.

Num primeiro momento, foram realizados testes de compressão a discos cilíndricos, como forma de caracterizar os diferentes materiais pelo seu módulo de Young ( $E$ ). No corrente projeto, 3 materiais (2 resinas epoxídicas e um silicone) foram considerados como forma de simular o comportamento do calo. Os resultados indicam valores de  $E=6$  MPa,  $E=100$  MPa e  $E=300$  MPa, o que permitiu caracterizar duas diferentes fases de consolidação do calo ósseo. Além disso, testes de compressão foram realizados para estudar o comportamento da tíbia em diferentes fases de cicatrização quando sujeita a uma série de cargas de compressão. A implementação de um extensómetro em cada uma das barras do fixador comprovou que este largamente contribui para a acomodação da carga ao longo do processo de consolidação. Essa contribuição alivia à medida que o calo consolida e aumenta o seu módulo de Young.

Um modelo tridimensional de elementos finitos da tíbia com um fixador acoplado foi criado recorrendo a uma análise de imagiologia à superfície da tíbia e à medição de um fixador externo regular. Dois modelos tridimensionais da tíbia, assumindo uma distribuição em três camadas (osso cortical, osso trabecular e canal medular), com uma fratura transversal e uma oblíqua foram considerados. O processo de cicatrização foi simulado considerando um calo de

diferentes propriedades mecânicas. As tensões de Von Mises foram o parâmetro escolhido para a avaliação dos resultados nas 3 principais regiões: calo, osso e barra do fixador. O resultado da análise dos elementos finitos permitiu corroborar as conclusões assumidas pelos ensaios de compressão e permitiu uma comparação quantitativa entre as tensões em cada secção.

A vantagem que este projeto poderá trazer para a comunidade médica prende-se com a possibilidade de avaliar quantitativamente o processo de consolidação da fratura, sendo desnecessário sujeitar o paciente a radiações prejudiciais ou intervenções cirúrgicas desnecessárias.

**Palavras-chave:** Tíbia, calo, fratura, fixador externo, ensaios mecânicos de compressão, análise dos elementos finitos, simulação, biomecânica.

# Abstract

Human tibial fractures are one of the most frequent bone fracture, due to its wide surface area. Its main function lasts with the purveyance of equilibrium and support to the body. Bone fractures in lower limb's long bones are complex lesions that commonly results in long disability periods. After a fracture occur, there are multiple approaches to perform the bone fracture immobilization. The external fixation has traditionally been used in closed fractures and when the risk of infection is high, providing sufficient rigidity and stability to align the fractured bone. The currently systems only allows the analysis of the consolidation progress through X-rays, what difficult the continuous system evaluation. Moreover, there are significant drawbacks to the patient, especially the exposure to radiation, and depends on the skills of the operate. This thesis intends to monitor the bone consolidation process by undergoing mechanical compression tests, as well as creating a numerical model which simulates their behaviour and predict bone regeneration.

In a first stage, compression tests of cylindrical discs were performed to characterize different materials by its Young' modulus (E). In the current study, three materials (two epoxy resins and a silicon) were considered to simulate callus behaviour. The results indicate values of  $E=6$  MPa,  $E=100$  MPa and  $E=300$  MPa, what allow to characterize two different callus' consolidation phases. Furthermore, compression tests were performed to study the behaviour of the tibia in different phases of healing when subjected to a set of compressive loads. The implementation of strain gauges in the two external fixator's rods prove that the fixator system broadly contributes to the load accommodation along the consolidation process. That contribution reduces as the callus consolidate and increase its Young's modulus.

A 3D finite element model of the tibia with fixation was created resorting to imaging surface analysis of the tibia and measurement of a regular external fixator system. Two 3D models of the tibia, focused in a three-layer structure (cortical bone, trabecular bone and medullary canal), with a transversal and oblique fracture was considered. The healing process was simulated considering a callus with different mechanical properties. Von Mises stress were chosen as parameter for the evaluation of the results in three main regions: callus, bone and

fixator's rod. FEA results corroborate the conclusions taken in the compression tests and allow a quantitatively comparison between sections' stresses.

The advantage that this project could bring to the medical community lasts with the possibility to evaluate quantitatively the fracture consolidation process, being unnecessary to subject the patient to harmful radiations or unneeded surgical interventions.

**Keywords:** tibia, callus, fracture, external fixator, compression mechanical tests, finite element analysis, simulation, biomechanics.

# Acknowledgements

To Professor Mário Vaz, for all the guidance and availability along the execution of the project.

To Carla Lopes, for all the assistance, advices and patience in the execution of every steps of the dissertation.

To LOME and LABIOME, for all the resources that put at my disposal.

To all my friends that encourage me to present a remarkable project within the time limits.

To my best friend, and girlfriend, Inês, for being the everyday reminder that the best things in life appear with hard work and when is less expected.

To all my family, giving special emphasis to my parents and brother, for being my true inspiration in life, each one in a different manner. Love you!

Thank you!





# Index

Resumo.....	iii
Abstract.....	v
Acknowledgements .....	vii
Figures List.....	xiii
Tables List.....	xix
Abbreviations and Symbols .....	xxi
Chapter 1. Introduction.....	23
1.1. Objectives .....	23
1.2. Structure of the Thesis.....	24
Chapter 2. Osteology of the Tibia.....	27
2.1. Skeletal System.....	27
2.1.1. Anatomical position and reference axis .....	28
2.1.2. Lower Limb .....	29
2.1.3. The Tibia .....	31
2.2. Bone tissue .....	34

2.2.1. Cancellous bone.....	34
2.2.2. Cortical Bone .....	35
2.2.3. Osteogenesis - Intramembranous Ossification .....	36
2.2.4. Osteogenesis - Endochondral Ossification .....	37
2.3. Fracture.....	38
2.3.1. Fracture repair .....	39
2.3.2. Consolidation Time .....	40
2.3.3. Solution procedure .....	41
2.3.4. External Fixation.....	42
2.4. Load sensors.....	45
2.5. State of the Art.....	46
2.5.1. Using Percussion Signals .....	47
2.5.2. Measuring Bending Stiffness .....	49
2.5.3. Using Ultrasonic Waves .....	50
2.5.4. Load Cell Transfer Function .....	52
Chapter 3. Biomechanics of the Tibia .....	53
3.1. Biomechanical Principles .....	53
Chapter 4. Finite Elements Modelling .....	57
4.1. Finite Elements Method Evolution.....	57
4.2. 3D Modelling of the Tibia .....	58

4.2.1. Obtainment of the three-dimensional geometry.....	58
4.2.2. Finite Elements Mesh .....	63
4.2.3. Constitutive Model and its mechanical properties.....	66
4.2.4 - Load and Boundary Conditions .....	67
Chapter 5. Experimental Tests .....	69
5.1. Samples Characterization.....	69
5.1.1. Materials used .....	69
5.1.2. Materials characterization test.....	71
5.1.3. Samples' characterization results .....	74
5.1.4. Callus' characterization .....	76
5.2. Compression Test.....	77
Chapter 6. Results Presentation.....	81
6.1. Results of the Finite Element Analysis .....	81
6.2. Results of the Compression tests.....	89
Chapter 7. Conclusion and future work .....	93
7.1. Conclusion .....	93
7.2. Future work .....	94
References .....	95
Annex.....	99



# Figures List

Figure 1. Human male skeleton: (a) Anterior and (b) posterior views of the Human Male Skeleton [3].	27
Figure 2. Anatomical Position and respective planes (adapted from [8]).	29
Figure 3. Scheme of the axial (a) and appendicular (b) skeletons [3].	29
Figure 4. Anterior (a) and Posterior (b) views of the Lower Limb [3].	30
Figure 5. Landmarks of a long bone disposition [2].	31
Figure 6. Right tibia: (a) Anterior and (b) Posterior views [3].	32
Figure 7. Tibial upper epiphysis [9].	32
Figure 8. Bony Landmarks of tibial shaft [9].	33
Figure 9. Cancellous bone structure [11].	34
Figure 10. (a) Cortical bone scheme and (b) histological image (adapted from [2]).	35
Figure 11. Diagram describing intramembranous ossification (adapted) [13].	37
Figure 12. Diagram of endochondral ossification [14].	38
Figure 13. Types of bone fractures [14].	39
Figure 14. Inflammatory response scheme [16].	40
Figure 15. Tibial fracture treated with open reduction an internal fixation using plates [20].	42

Figure 16. External fixator's assembly scheme [20].	43
Figure 17. Strain gages [24].	45
Figure 18. Wheatstone bridge scheme [24].	46
Figure 19. Intact bone p-note [25].	47
Figure 20. P-note's frequency spectrums [25].	48
Figure 21. P-note's temporal Spectrums [25].	48
Figure 22. Bending stiffness measurement apparatus [26].	49
Figure 23. Load-Deformation relation [26].	50
Figure 24. System's architecture [27].	51
Figure 25. (a) Transmitted signal, (b) signal received, after surgery, (c) signal received, during consolidation [27].	51
Figure 26. System's architecture [28].	52
Figure 27. Types of loading that a long bone is subjected [31].	54
Figure 28. Strain scheme [32].	55
Figure 29. Stress-strain curve for cortical and cancellous bones (adapted from [33]).	56
Figure 30. Tibia 3D model: posterior(a) and anterior(b) views.	59
Figure 31. Tibia model dimensions.	59
Figure 32. Distal Epiphysis' inferior view.	60
Figure 33. Tibial model sections.	61
Figure 34. a) Tibia with 30° fracture b) 30° fracture with callus c) Tibia with transversal fracture and d) transversal fracture with callus.	61

Figure 35. Model of the fixated tibia with transverse fracture (a) and oblique fracture (b). .....	63
Figure 36. Tibia's components mesh. ....	64
Figure 37. Callus mesh. ....	64
Figure 38. External Fixator mesh, constituted by a rod (a) and pins (b). ....	65
Figure 39. Proximal (a) and Distal (b) frames' mesh. ....	65
Figure 40. Load applied in the transverse fractured bone model. ....	68
Figure 41. Boundary conditions in proximal and distal regions of the transverse fractured bone model. ....	68
Figure 42. Epoxy Resin (a) and Silicon (b) samples. ....	70
Figure 43. The Gray sample. ....	71
Figure 44. Cylindrical shape mold. ....	72
Figure 45. (a) Instron EletroPuls E1000. (b) Compression test executed for the characterization of the Silicon sample. (c) Compression of the Epoxy Resin sample. ....	73
Figure 46. Force-displacement curve of cortical bone [55]. ....	73
Figure 47. Stress-strain curve for the samples under test. .... <b>Erro! Marcador não definido.</b>	
Figure 48. (a) Stress-strain curve for the bone sample (b) Bone sample. ....	76
Figure 49. Bone and external fixator model, with strain gauges coupled. ....	79
Figure 50. Test setup. ....	79
Figure 51. Sections under analysis: callus, bone section surrounding the fracture and callus. .....	81
Figure 52. Representation of the Von Mises variation during transverse callus' regeneration. .....	82

Figure 53. Von Mises stress distribution (MPa) when transverse callus has a Young's modulus of (a)3MPa, (b)250MPa, (c)750MPa, (d)1500MPa and (e)6000MPa. ....	83
Figure 54. Von Mises stress distribution (MPa) at Rod when transverse callus' has a Young's modulus of (a) 3MPa, (b) 250MPa, (c) 750MPa, (d) 1500MPa and (e) 6000MPa. ....	84
Figure 55. Bone's upper interface with callus stress distribution when transverse callus' has a Young's modulus of (a)3MPa, (b)250MPa, (c)750MPa, (d)1500MPa and (e)6000MPa. ....	85
Figure 56. Transverse callus' and Bone's Von Mises graph final phase behaviour. ....	86
Figure 57. Displacement variation during transverse callus' regeneration. ....	87
Figure 58. Representation of the Von Mises variation during oblique callus' regeneration. ....	87
Figure 59. Displacement variation during oblique callus' regeneration. ....	88
Figure 60. Denomination of the Strain Gauges. ....	89
Figure 61. Strain Gauges' measurements in the compression test of the Tibia model. ....	90
Figure 62. Von Mises' distribution for a transversal fracture with a Young's modulus of 3 MPa. Fixator's rod at the top; callus in the middle; bone structure down. ....	99
Figure 63. Von Mises' distribution for a transversal fracture with a Young's modulus of 250 MPa. Fixator's rod at the top; callus in the middle; bone structure down. ....	100
Figure 64. Von Mises' distribution for a transversal fracture with a Young's modulus of 750 MPa. Fixator's rod at the top; callus in the middle; bone structure down. ....	100
Figure 65. Von Mises' distribution for a transversal fracture with a Young's modulus of 1500 MPa. Fixator's rod at the top; callus in the middle; bone structure down. ....	101
Figure 66. Von Mises' distribution for a transversal fracture with a Young's modulus of 6000 MPa. Fixator's rod at the top; callus in the middle; bone structure down. ....	101
Figure 67. Von Mises' distribution for an oblique fracture with a Young's modulus of 3 MPa. ....	102



Figure 68. Von Mises' distribution for an oblique fracture with a Young's modulus of 250 MPa. .....	102
Figure 69. Von Mises' distribution for an oblique fracture with a Young's modulus of 750 MPa. .....	102
Figure 70. Von Mises' distribution for an oblique fracture with a Young's modulus of 1500 MPa. ....	103
Figure 71. Von Mises' distribution for an oblique fracture with a Young's modulus of 6000 MPa. ....	103



# Tables List

Table 1. Types of external fixation (adapted from [23]). .....	44
Table 2. Dimensions of components of the fixator model (based in the Hoffman 3 external fixator)[41].....	62
Table 3. Mechanical properties of tibia and components of external fixator. ....	66
Table 4. Callus properties in the various stages[45].....	67
Table 5. Altpol rubber samples [48]. .....	70
Table 6. Calculated Young's modulus for the samples under test. ....	75
Table 7. Materials' assignment to their respective callus' phase. ....	77
Table 8. Synthetic bone measurements [39]. .....	78



# Abbreviations and Symbols

HSC	Haematopoietic stem cells
MSC	Mesenchymal stem cell
FEM	Finite Element Model
FEA	Finite Element Analysis
CT	Computed Tomography
3D	Three-Dimensional
F	Load
N	Newton
A	Area
$\varepsilon$	Strain
E	Young's modulus
$\sigma$	Stress
Pa	Pascal
mm	Millimetre
Cm	Centimetre
Min	Minute
s	Second



# Chapter 1. Introduction

Biomedical Engineering results on a symbiosis between mechanics or physics laws with the physiological comprehension of the human body and its motion study. The application of the biomedical engineering, through Biomechanics, to the biological systems' study allows the comprehension of the movement and loads generated in the living tissues, what enables the implementation of conceptual and mathematical tools that can predict its behavior.

In the past years, the characterization of fractures has been a very demandable subject. As each patient has a different tissue regeneration behavior, the monitoring of the consolidation process allows the comprehension of the risk factors and to infer the treatment duration. The rehabilitation time is associated with direct costs due to the medical action, and indirect costs associated to the immobilization time. In that way, the better understanding of the mentioned physiological process could optimize the recovery by reducing costs and improve the treatment in order to scaffold the bone to a more effective growth.

## 1.1. Objectives

There is a certain complexity in the biomechanical and biological investigation of the bone fracture consolidation mechanisms. It isn't already fully-known the way that osseous tissue reacts to external stimulus, auxiliary artificial apparatus or materials used, leading to an open area to be explored and discovered.

The main objective is to study the bone consolidation process through the calculation of mechanical properties of the tibia, more specifically those who can affect the regeneration, for example rigidity or stress. In that way, starting on the global mechanical behaviour of the osseous structure, it is possible to evaluate the properties on the fracture's interface area, and infer the progression state of the bone consolidation process. That purpose may be fulfilled through an approximation of a finite element analysis and a mechanical axial compression test

executed on a reliable tibia model. The biomechanical variables could be compared in order to complement each other in the quest for an optimized recovery and surgical procedure.

The present work will be written for the achievement of the master's degree in Bioengineering, and results of a collaboration between the Laboratory of Optics and Experimental Mechanics and the Orthopaedics and Traumatology's Service of São João Hospital Centre. Given the diverse subjects of interest of each unit, we can count on a synergy of a multidisciplinary investigation group, that grants a wise overview over each task, to enable a sequential multiscale study.

The project will be organized into three major stages:

- In the first phase, the proposal is to create the bone structure and the respective external fixator, using a CAD software: to attain a precise design of the bone geometry, some medical imaging techniques can be used. When the bone/fixator system is complete, it can be imported into a Finite Element Analysis software -ABAQUS® -, simulating all the interface generated strain, proposing an adequate correlation of the osseous matter's behaviour when subjected to external stimulus;

- The next stage focuses on the creation of an in-vitro model using a Synbone model to allow the previous obtained principle validation. The intention is to construct a data collection system based on a strain gauge, capable of measure the deformation, and incorporate it on the synthetic bone under test conditions that mimics the usual efforts that a common fractured bone is exposed;

## 1.2. Structure of the Thesis

This thesis is organized in seven chapters:

### Chapter 1. Introduction

It is introduced the dissertation theme subject, being defined the main objectives and the thesis' structure.



## **Chapter 2. Osteology of the Tibia**

In this chapter, it is made a succinct description of the anatomical plans' terminology, as well as the general anatomy of the Tibia and the osteogenesis mechanism that results in different bone components. A brief explanation of the fracture repair process and external fixator system is also mentioned. The chapter ends with two subchapters dedicated to the Load sensors and to the State of Art that collects solutions to evaluate qualitatively the regeneration process when associated to an external fixator apparatus.

## **Chapter 3. Biomechanics of the Tibia**

In this section is mentioned some biomechanical principles associated to the bone, and introduced some formulas that will be taken into account to the results' treatment.

## **Chapter 4. Finite Element Modelling**

In this chapter it is intended to present the finite element method, providing a summary of its historical evolution, as well as its main characteristics. In this phase, it is explained the protocol of construction of the numerical simulation model, referring its three-dimensional geometry, its constitutive model, its mesh and its load and boundary conditions.

## **Chapter 5. Experimental tests**

In this section, it is made the characterization of a certain number of material samples, in order to characterize the callus' consolidation behaviour in each of its regeneration phases. After the mentioned characterization, some compression tests were realized in order to characterize the callus progression behaviour.

## **Chapter 6. Results presentation**

In this chapter it is presented the results obtained by the simulations in chapters 4 and 5.

## **Chapter 7. Conclusion and future work**

Lastly, it is exposed the main conclusions deduced by this project and future development suggestions to improve the results.



# Chapter 2. Osteology of the Tibia

## 2.1. Skeletal System

Human Skeleton represents about 18% of the human's body medium weight, distributed by its 206 bones, from head-to-toe. This system is the main foundation of the body, being responsible for some major attributes, and functions, that are endorsed in our physiology [1].

The skeleton is the primary subject that supports the body, maintains its shape and gives movement to human's framework and is represented in Figure 1. The association between bones and cartilage provides a well-shaped scaffold that maintains the living structures in his right relative and absolute position, despite the efforts they are subjected (gravity, atmospheric pressure, other external forces). If added ligaments' properties, muscles' points of attachment and tendons, bones also facilitate movement: acting as muscles' behaviour support structure, or transmitting muscle-produced forces, skeleton provides a biomechanical assist to human motility [2].

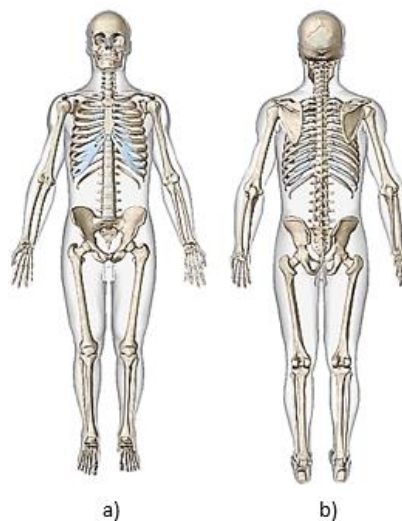


Figure 1. Human male skeleton: (a) Anterior and (b) posterior views of the Human Male Skeleton [3].

The skeletal system also provides protection from injury for vital internal organs, by cover or enclosing them [2].

Haematopoiesis is a process, that occurred in the bone, that is responsible for the production of vastly specialized blood cellular components, derived from haematopoietic stem cells (HSC). HSC nest in bone marrow, that is located on the core of bones. These cells are self-renew and multipotent, it means that they can differentiate into a considerable number of cell types, in this case blood cell types, being an important part of body's immune system [4].

The bone matrix can also store several minerals, especially calcium (Ca) and Phosphorus (P). In case of a deficit of those minerals in the bloodstream, they are released to maintain the concentration needed to the occurrence of physiological processes. Bones can also act as a reservoir of chemical energy on their adipose cells [2]

The bone is projected as the monomer of skeletal system. It is a rigid organ, presenting a collagen mainly constituted matrix that attends about 30% of its structure; the remaining 70% is filled with minerals that strengthen the structure, mainly hydroxyapatite (HA). The inorganic component confers toughness and rigidity to the bone, while the collagen-based organic one is responsible for its elasticity. The impermeability of the osseous matter is propitious to a high blood irrigation [5].

### 2.1.1. Anatomical position and reference axis

The anatomical position is a reference position that allows a directional and positioning concept in the description of a certain human body region. At first, a universal body position is assumed: standing, with the upper limbs extended along the body and the hands' palms faced forward, the lower limbs united and the chin perpendicular to the chest [6]. According to that position, there are several axis or planes that divides the body through imaginary planes in a certain direction, giving several designations to the resultant parts. The anatomical position and the referred plans can be seen in Figure 2.

It is also important to describe the nomenclature attributed to the resulting sides of an imaginary plane that divides transversally the bone. The proximal part expresses the side closer to the point of origin of a body part. The distal part, on the contrary, represents the side away from the trunk centre [7].

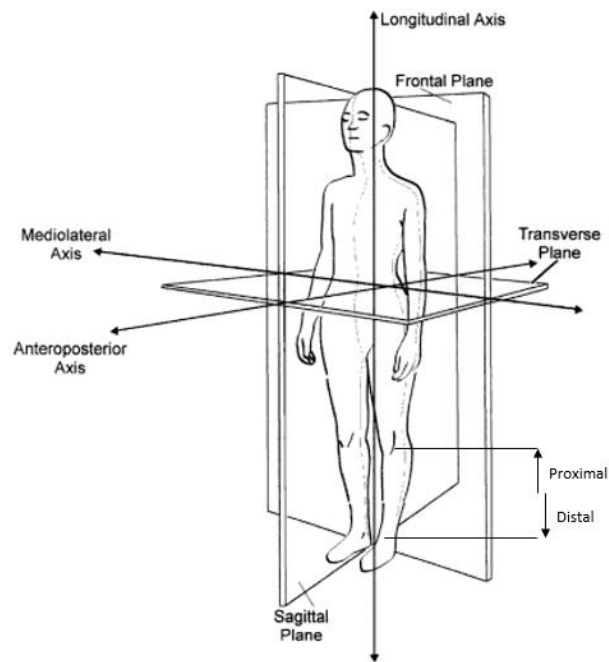


Figure 2. Anatomical Position and respective planes (adapted from [8]).

### 2.1.2. Lower Limb

Human skeleton can be sectioned into two parts: axial and appendicular skeletons. A schematic presentation of this division can be seen in Figure 3.

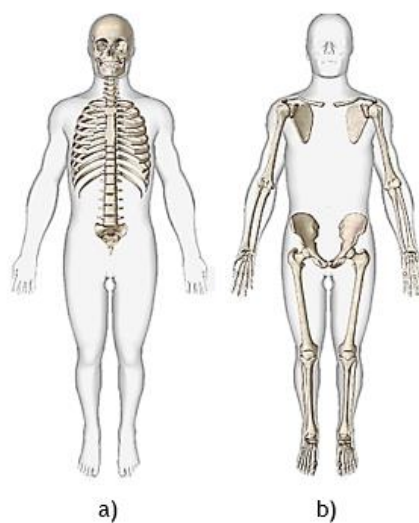


Figure 3. Scheme of the axial (a) and appendicular (b) skeletons [3].

Axial skeleton is composed by all the bones in the skull, and the bones that complete the vertebral column, making a total of 80 elements. The “Axial” term is referred to the relative position of these bones in the human body, covering the central vertical Axis of torso [9].

Appendicular skeleton includes all skeletal elements in the limbs, either superior or inferior, in the pelvis, and the shoulder formation. In total, the Appendicular Skeleton involve 126 bones. Despite the origin of the “Appendicular” term remits to the substantive “Appendix”, this section is responsible for the locomotion, body weight’s support and interaction with the surrounding environmental elements [9].

All the bones can also be classified according to their form. All skeletal elements in the human body own different functions, different shapes and different sizes, so it is foreseeable that the classifications will be divergent: long bones, short bones, flat bones, irregular bones, or sesamoid bones [9].

The lower limb is an appendage of the human body that greatly contributes to the body’s equilibrium and support, and allows the locomotion of the human being. With a grid that extends from pelvis to toe, this formation is composed by 62 bones [9], as is represented in Figure 4.

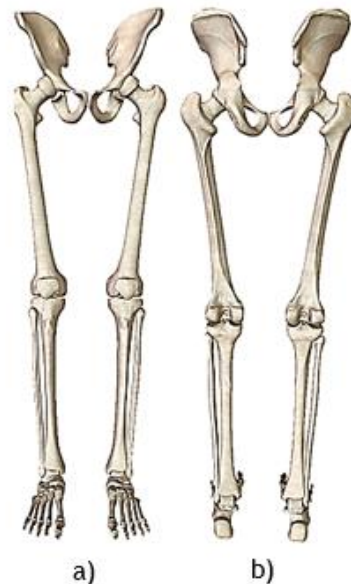


*Figure 4. Anterior (a) and Posterior (b) views of the Lower Limb [3].*

Cylinder-like shaped bones, with its length widely greater than its width, are named as long bones. These bones have a well-defined internal disposition: the periosteum, a connective tissue membrane, covers the radially peripheral shell of the cortical bone; below that shell, there is a cancellous bone layer, a honeycombed network that greatly boosts the mechanical properties of the bone, and provide a high internal blood irrigation for bone nutrition. That grid covers the medullary cavity, where dwells a semi-solid tissue from the immune system, the bone marrow [10], pictured in Figure 5.

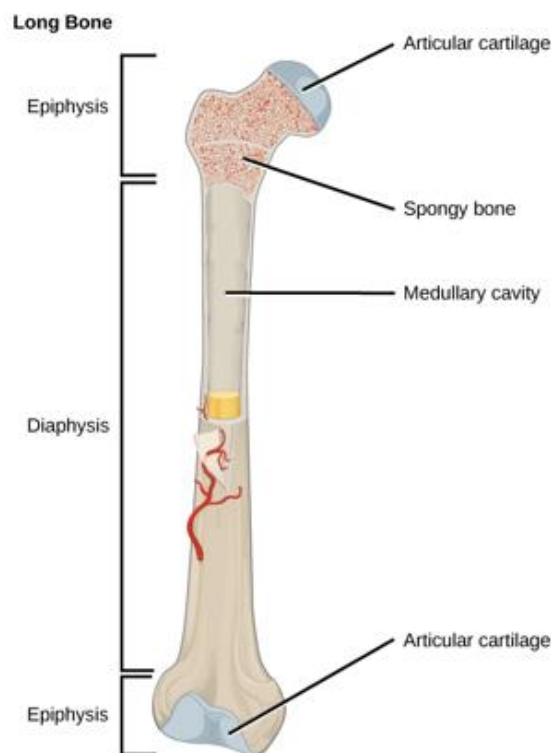


Figure 5. Landmarks of a long bone disposition [2].

The set of long bones that belong to the lower limb, excluding metatarsal bones, provide a set of three bones: femur, tibia and fibula.

### 2.1.3. The Tibia

Tibia is the largest and strongest bone in the human body, right after femur. In association with fibula, they form the skeleton of the leg. As tibia is the stronger between those, it is the

main mean of weight bearing in the leg, providing equilibrium and support to the body. The anterior and posterior views of the tibia are shown in Figure 6.

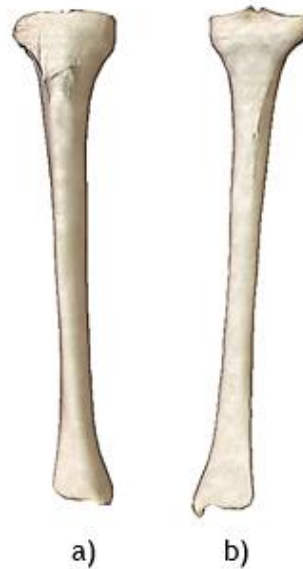


Figure 6. Right tibia: (a) Anterior and (b) Posterior views [3].

The regular partition of a long bone also applies to the tibia, with two epiphyses - proximal and distal extremities - and a diaphysis - the bony body named shaft, the structures are represented in Figures 7 and 8, respectively.

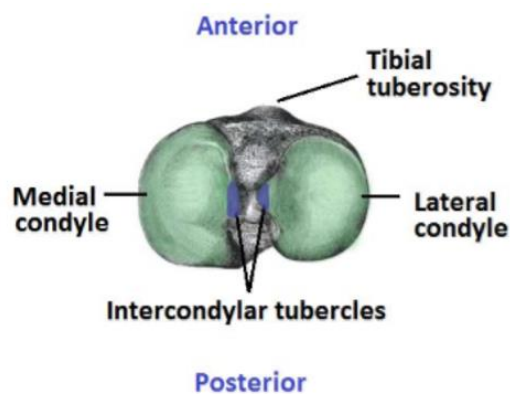


Figure 7. Tibial upper epiphysis [9].



Tibia also possesses two condyles in its proximal epiphysis, medial and lateral, that interact to their correspondent in femur's distal extremity. Between those structures, there is an intercondylar eminence, where the knee joint's ligaments and the menisci attach. The tibia is connected to the fibula by an interosseous membrane located laterally [9][10].

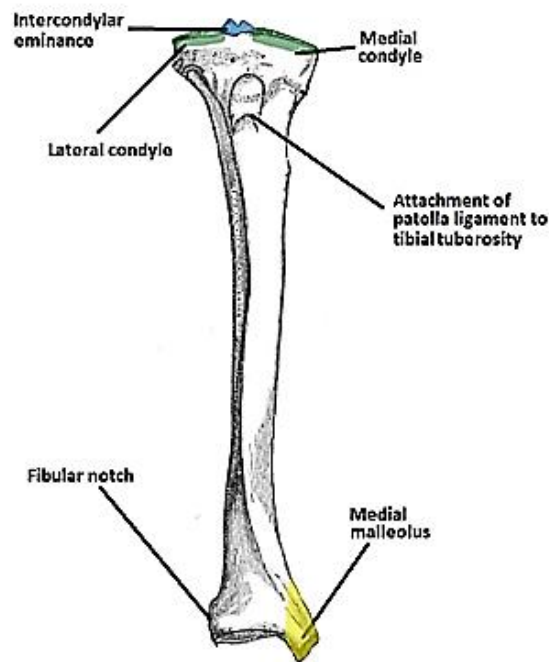


Figure 8. Bony Landmarks of tibial shaft [9]

Tibial shaft is a portion that has structures to meet its muscular and osseous needs, ending roughness and protruding bone projections to connect, in a lateral side, with fibula, and with the muscular architecture of the leg [10].

The lower part is a segment of the ankle joint, allowing an osseous medial protuberance—the medial malleolus, that propagate downwards till the talus. Laterally, there is the second point of attachment to the fibula, the fibular notch, constituting the lateral malleolus to bind the ankle joint [10].

Despite the stiffness of the tibia, fractures may occur. In the leg, a fissure in tibia's shaft can be functionally supported by an intact fibula, as long as the process of bone regeneration doesn't take too long. In the epiphysis, the injuries are most likely to exist, because is a place of a high concentration of soft tissues [10].

## 2.2. Bone tissue

Bone tissue is a branch of the connective tissue with some unique properties, and can be subdivided into two different types, located in different morphological regions in the bone: cancellous bone and cortical bone [4].

### 2.2.1. Cancellous bone

The cancellous bone is a set of tissue bridges in a three-dimensional net, giving rise to macroscopically visible cavities filled with regular connective tissue. The cancellous bone matrix possesses some gaps, as is represented in Figure 9. In these holes, are inserted osteocytes, a fully grown and differentiated bone tissue cell, that allows a correct regulation of calcium levels in neighbourhood.

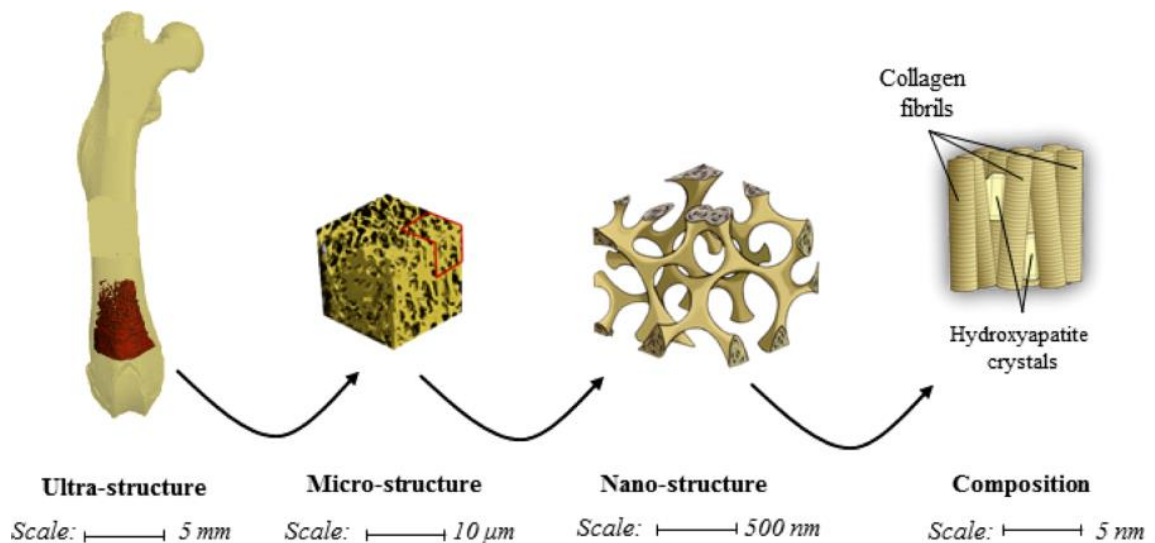


Figure 9. Cancellous bone structure [11].

It is foreseen the fluidity and constant renovation of this structure. That attributes are ensured by osteoblasts: located in the limit of the matrix, those mononuclear cells promote bone synthesis, through the formation of organic components that are part of bone matrix, like collagen, proteoglycans and glycoproteins. The renovation cycle also presupposes a mean of

bone tissues' reabsorption, reaching an equilibrium state, ensured by osteoclasts. Those last results from connective tissue's digestive cells, named macrophages [4][5].

The ambition of renovate and remodel the bone matter is to regulate calcium levels, repair microfractures due to everyday stress and fatigue, and to assemble an ideal skeleton silhouette along the normal body's growth throughout life.

### 2.2.2. Cortical Bone

The cortical bone corresponds to the longer and more longitudinal segment of any bone, arranged in a pattern of bone tissue with tubes of successively lower gauge - the Haversian Canal, that is considered cortical bone's functional unit. The referred system, composed from spiralized-arranged organic collagen and inorganic matter as calcium, is a site where the blood vessels and some nervous cells proceed their way through the body, in order to vascularize and nourish all bone tissue (an essential feature, due to its intrinsic impermeability). The structure is represented in Figure 10.

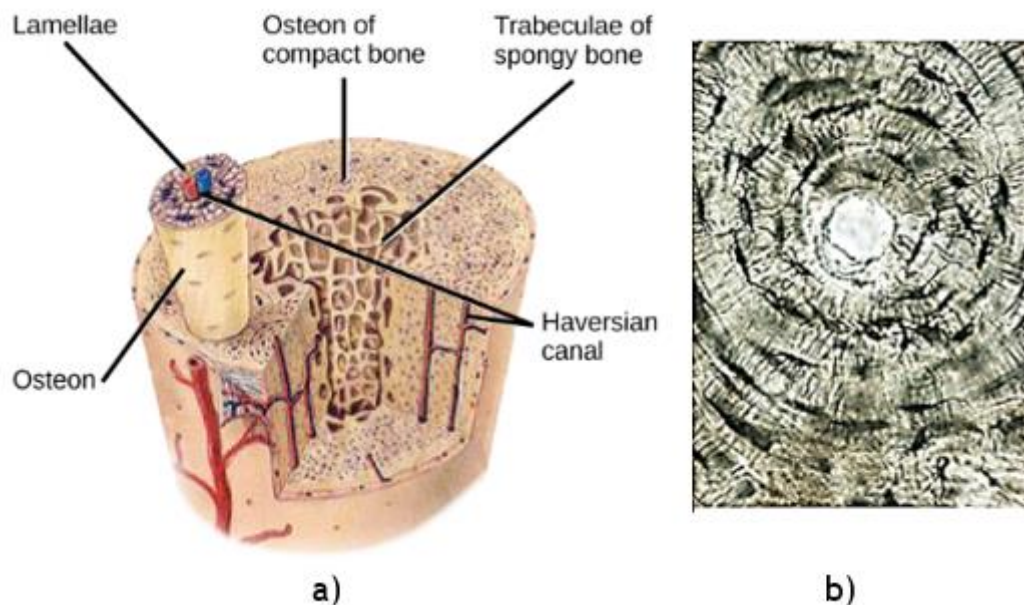


Figure 10. (a) Cortical bone scheme and (b) histological image (adapted from [2]).

Inside the Haversian structure, the presence of another cells are also notorious: osteoblasts and osteoclasts located, as in cancellous bone, near the limit. Furthermore, is unavoidable the existence of a configuration that allows the communication between Haversian's covers, locus of bone cells, and its channel, where all vessels pass: the Volkmann's Channels [5].

### 2.2.3. Osteogenesis - Intramembranous Ossification

As invoked previously, bone tissue is regularly renewed through a process called osteogenesis. There are two main modes of bone formation: intramembranous ossification and endochondral ossification. Both required the conversion of a pre-existing mesenchymal tissue into bone tissue. They diverge on the existence of a cartilaginous intermediate: intramembranous ossification assumes a direct conversion of mesenchymal tissue into bone; endochondral ossification employs the same scheme, but with the medial formation of a cartilaginous matter [5].

A mesenchymal stem cell (MSC), is a multipotent stem cell, native from an embryonic tissue, that as the capacity to differentiate into a variety of cell types.

Intramembranous ossification, named over its occurrence between membranes, is the main mechanism during foetal development by which the bones of the skull are formed. The process begins with the morphological and configurational transformation of the MSC to become osteoblasts. Osteoblasts can secrete Type-1 Collagen, principal component of extracellular matrix, and input it the power to bind calcium salts, proceeding to the calcification of the just-created matrix. When all the ossification centres start to emerge, forming a net of miss-oriented collagen fibers, and the trapped MSC evolves to osteoblasts, is formed the Primary Bone Tissue. The perforation from blood vessels and the correct parallel orientation of the collagen fibers result in the formation of new cortical bone [2][12], as it is represented schematically in Figure 11.

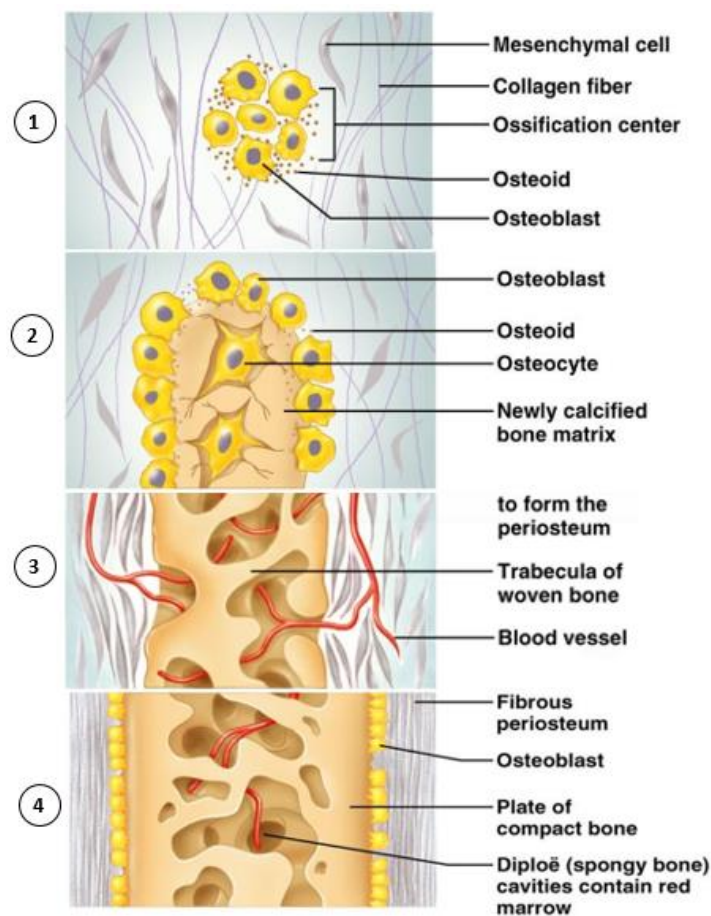


Figure 11. Diagram describing intramembranous ossification (adapted) [13].

#### 2.2.4. Osteogenesis - Endochondral Ossification

Endochondral ossification usually occurs in long bones, and it is associated to the genesis of cartilaginous tissue from aggregated MSC. In this case, modifications in MSC's morphology and shape result in a differentiate state into Chondrocytes. These cells are the basic unit of production and maintenance of the cartilage's matrix, being able to produce Collagen and Proteoglycans. Also, Chondrocytes secretes angiogenic factors responsible to the formation of blood vessels, future means of irrigation of the new bone tissue. With the flow in these vessels, some osteoprogenitor cells and HSC arrive to the osteogenic centre, and stimulates its differentiation into osteoblasts. The existence of a bone's matrix production cell and the calcification of the pre-existing tissue, encourage Chondrocyte's apoptosis and the synthesis of bone matrix. Thereby, the cartilaginous intermediate becomes a rudimentar cancellous bone [12], as shown in Figure 12.

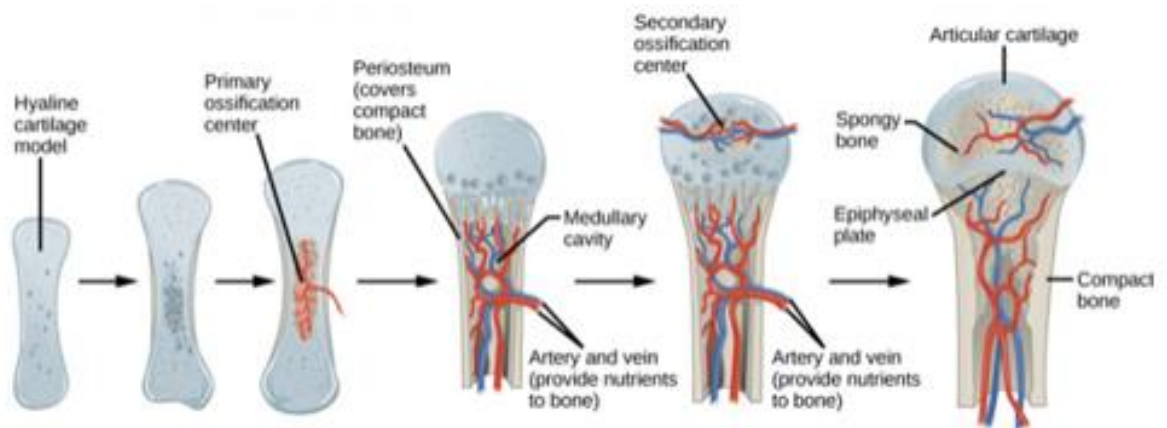


Figure 12. Diagram of endochondral ossification [14].

### 2.3. Fracture

Although bone stiffness is evident, the human skeleton is still susceptible to fractures, especially in the long bones. A hard strike conjugated with an effective impact orientation can lead to several traumas, like bone bending, cracking or snapping. The person's condition and age is also a fact considered; it's quite evident that an aged individual is more disposed to an aggravated event, with serious complications, than a baby. With age, bone matter becomes fragile and feeble, carrying severe effects to a heretofore minor trauma; also, several conditions, as osteoporosis, increase the risk of low-impact lesions [15].

Bone fractures are the result of an impact whose magnitude applied is superior than its resistance and elasticity coefficient. This lesion leads to a loss on bone continuity and a scant bone support.

A closed fracture is obtained when the broken bone doesn't cleave the skin; on the other hand, if it happens is considered an open fracture. In the cases where the skin is not pierced, distinct events may develop: a simple break across the bone- transverse fracture -, a bone twisted apart - causing a spiral fracture, or a crushed bone - resulting in a comminuted fracture [15]. A representation of the previous mentioned closed fractures is represented in Figure 13.

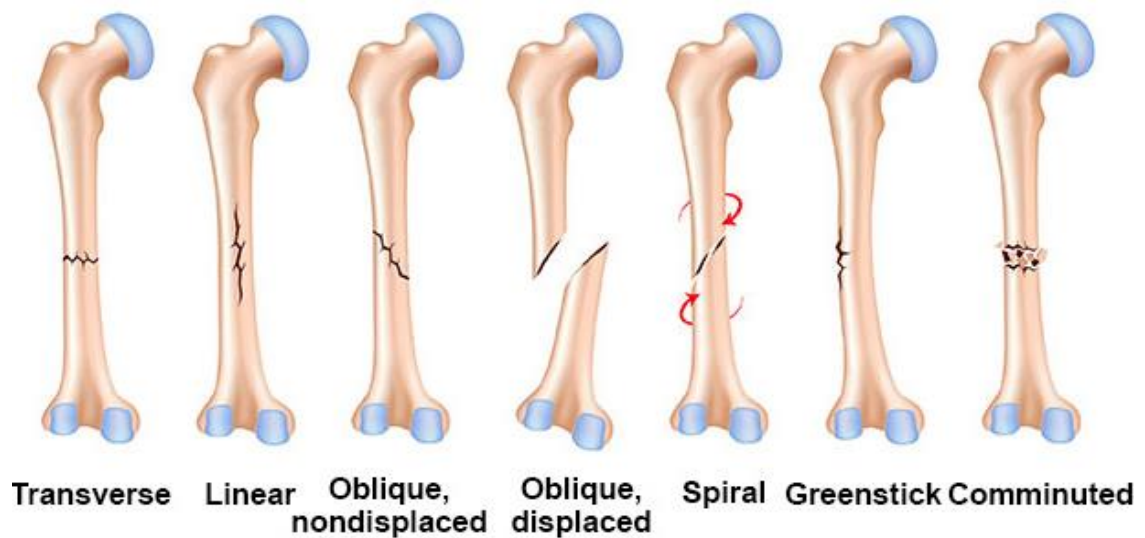


*Figure 13. Types of bone fractures [14].*

Due to the high blood irrigation of the inner bone, bleeding is a regular problem associated to the fracture. The high amount of surrounding blood causes periosteum dilation, which is stocked with nerve endings, that causes pain on the occurrence of any movement or touch. An interruption of the bone's blood supply can lead to necrosis of the osseous cells, due to the scarce oxygen concentration [15].

### 2.3.1. Fracture repair

Fracture repair can be divided into three partially overlapping stages: inflammatory response, repair and remodelling phases. It is a sequential tissue differentiation process that is characterized by a callus formation, where both intramembranous and endochondral ossifications take place [15][16].

Disruption of the blood flow leads to the appearance of hypoxic areas, due to the ineffective supply of oxygen and nutrients in the fracture site. The presence of a large amount of necrotic material and blood clots elicits a sharp inflammatory response to suppress aggravated effects. That reaction starts with vasodilation and plasma exudation, causing an edema in the affected area, followed by the migration of immune system cells that clean up the debris from the fractured site. After the wound neat, is created a primary non-calcified new tissue to bound and give consistency to the fractured zone.

The ossification takes place in the repair phase, arousing calcification to evolve the created tissue to a harder and more resistant one. Intramembranous ossification occurs mainly in periphery forming a hard callus, while a soft callus is produced centrally by the means of an endochondral ossification. In this stage, osteoblasts' role is preponderant, creating a new calcified extracellular matrix. The repair stage lasts until bone has bridged the fracture site.

The remodelling phase involves an equilibrium of hard callus reabsorption and lamellar bone deposition. The process ends up when the tissue recovers all its biomechanical, physiological and physical features and properties [15] [16]. Figure 14 shows the tissue response to a fracture of the bone.

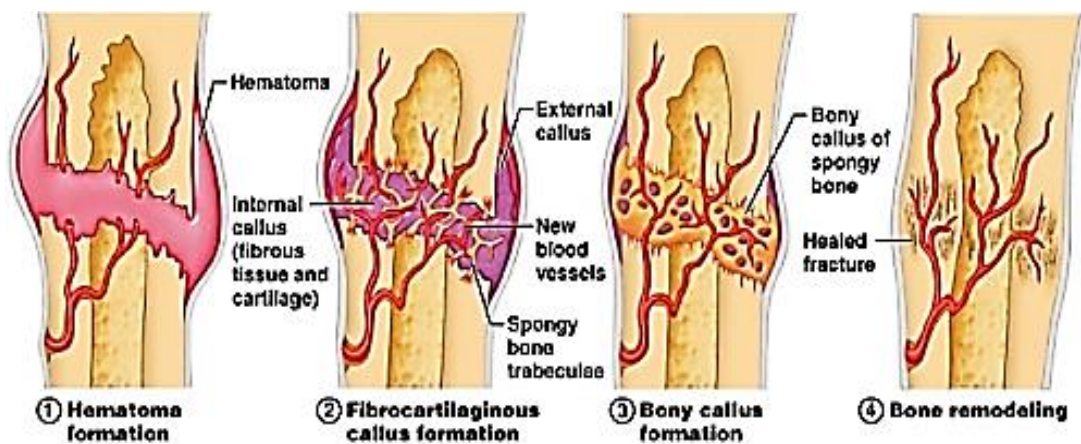


Figure 14. Inflammatory response scheme [16].

### 2.3.2. Consolidation Time

In the healing procedure, timing is essential to optimize the recovery, reducing disability time and its implied direct or indirect costs. If, for example, an external fixator is removed before the tibia reaches a satisfactory degree of consolidation, it can occur an extended disability, fixation failure or a deviation in the bone alignment. The parameter that appraises the degree of recovery is fracture union assessment, beyond muscle strength evaluation or joint mobility, which are only regained later in the healing process. Union is determined by the time when the patient can walk without notorious pain, fracture motion is non-existent and radiographs prove the continuity in the osseous structure. A controlled recovery plan is mandatory throughout all the process, establishing the appropriated external support and activity restrictions, in order to stimulate bone regeneration and prevent some sort of atrophy. Patients with union fractures



diagnosed are capable to bear full weight without external aid. As understandable, more severe traumas result in long healing time periods [17].

According to Ellis Series, the evaluation of displacement, comminution and wound severity in a tibial shaft fracture categorizes it into one of three severity grades: minor, moderate and major. Minor severity indicates an irregular displacement or angular deformity; in a moderate severity lesion there is a complete displacement with a minor comminution; and a major severity fracture represents all of those with denoting comminution or an open lesion [18].

Resorting to the gradation impose by Ellis, it is possible to differ the anterior mentioned classification using the average recovery time. For a minor severity fracture, it was needed 12 weeks for 80% of the patients present a healed fracture. For the moderate severity, it lasts 15 weeks to achieve that degree of recovery; and 27 weeks for a major severity trauma [17].

### 2.3.3. Solution procedure

To obtain the diagnosis and future proper treatment, an X-Ray examination is required. Nevertheless, to perform first-aid assistance, some circumstances can be subjective measured, like the pain revealed, the inability to move, the wound, or the bone alignment.

In an open fracture or an aggravated close one, an “open reduction and internal fixation” is mandatory: that means that an invasive surgery is required to realign the bone into its normal position, resort to steel screws, rods and plates, to stabilize the bone structure and to serve as a scaffold for bone healing. Additional complications can accrue from an exposed wound, like risk of infection, high blood loss or a complex soft tissue injury [19].



*Figure 15. Tibial fracture treated with open reduction an internal fixation using plates [20].*

Close fractures normally are treatable with a non-invasive “close reduction”, whose motto is to realign the bone to its ideal position. If the process objective is not achieved, or the location is not attainable, a surgery is needed. One approach is the use of an external fixator to guide the bone orientation and posterior healing process [19].

The fixation process involves four main principles that should be kept regardless the lesion severity or trauma: an anatomic reduction, to preserve the bone length and to restore the bone alignment and rotation; an adequate biomechanical stability helping in the body support function; the preservation of the blood flow, in order to favour the bone consolidation; and finally the muscular and articular mobilization, avoiding atrophies of any kind [19].

#### 2.3.4. External Fixation

External fixation is a surgical procedure to immobilize bone structures around the wound, allowing higher stability and an effective healing process. Holes are opening in upstream and downstream regions of the lesion and pins or screws are placed into them; out the physiological environment, an external frame, composed by metal bars and rods, joins the pins to make a rigid support. An example of the use of a fixator to immobilize a fracture is shown in Figure 16. It is required a regular maintenance to preclude infection events. External fixation is a minimally invasive quick process, but it is normally performed under a general anaesthesia.

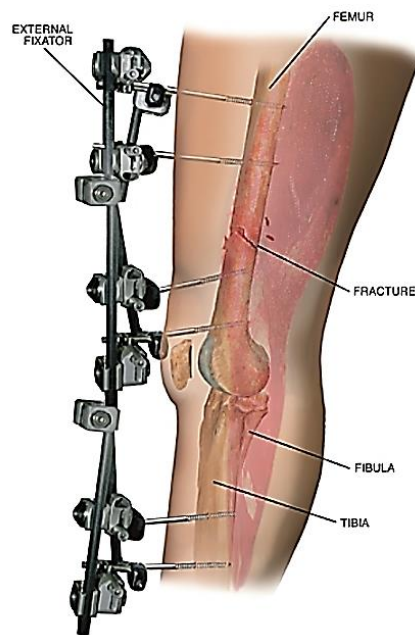


Figure 16. External fixator's assembly scheme [20].

The external fixator ensures a stable environment for bone regeneration, granting an adequate compression and distension, to resist to axial, shear and bending stresses. After the implantation of the metal structure, physiotherapy can begin immediately, to prevent muscle atrophy and to stimulate bone growth and mobility. Rehabilitation can take for about 6 months. Common conformations of assembly the fixator include Ilizarov and X-Fix [21].

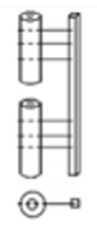
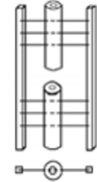


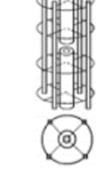

The cases where the fixator applies are related to the Tscherné classification: a system to labelling soft tissue injuries, differing on its severity and if it is an open or close one. So, the choice of an external fixator and its conformation are bond with the magnitude of the trauma and with the soft tissues affected [21].

Although there are several assembly conformations and concordant elements' size and shape, the materials used in the base components are well defined: bolts (including Schanz Pin), nuts and bars are usually made from a stainless steel, with high strength and corrosion resistance properties; all the connectors and stems are built from an aluminium alloy, a compound with high resistance, durability and lightness [21].

There are more than one thousand external fixation constructions available, with similar components used in different configurations. An external fixator can be classified into linear, circular or hybrid one. Each external fixation device can be also included in one of the six frame

types existent: each type has features inherent to a certain construction, or a combination of properties of both linear and circular fixators, intended as the hybrid ones. The external fixators are adjudicated to a certain type due to the characteristics of fixation, namely the insertion of transosseous elements in the injured bone, the biomechanical conditions and its actuation zones between bone fragments and the quantity and quality of the locals of bone formation [22]. The main aspects of each type of external fixation can be seen in Table 1.

Table 1. Types of external fixation (adapted from [23]).

Type	Examples	Features	Scheme
I. Monolateral	Hoffman, Lambotte, AO/ASIF	<ul style="list-style-type: none"> <li>- Pins capture both cortices but do not pass completely through the bone;</li> <li>- Transosseous elements installed in one plane and on one side.</li> </ul>	
II. Bilateral	Hoffman, Charnley	<ul style="list-style-type: none"> <li>- All transosseous elements are installed in one plane and pass through both cortices;</li> <li>- Longitudinal bars in each side to connect the transosseous elements</li> </ul>	
III. Sectorial	AO/ASIF, SKID	<ul style="list-style-type: none"> <li>- Pin placement limited to sector <math>\alpha</math> (<math>0^\circ &lt; \alpha &lt; 180^\circ</math>);</li> <li>- Do not include the insertion of true transfixation transosseous elements. Only wires and half-pins.</li> </ul>	
IV. Semicircular	Hoffman-Vidal, Fischer	<ul style="list-style-type: none"> <li>- External supports geometrically form sector <math>\beta</math> (<math>180^\circ &lt; \beta &lt; 360^\circ</math>).</li> </ul>	
V. Circular	Ilizarov, Kalnberz	<ul style="list-style-type: none"> <li>- Existence of external connecting rings and bars that surround the limb.</li> </ul>	
VI. Hybrid	Biomet hybrid external fixator, OrthoFix hybrid external fixator	<ul style="list-style-type: none"> <li>- Can combine all the feature of types I - V.</li> </ul>	

## 2.4. Load sensors

When an object is subjected to the action of a load it undergoes deformation. This deformation depends on the value of the load and also on the mechanical properties of the object. If a reference distance is previously defined on the surface of the object by two-point marking, it is possible to access the strain on the surface through this direction by comparing this distance with the initial one. In this way it is possible to obtain a signal proportional to the load, so it is possible to access the value of the applied force. The Load Sensor is a force transducer responsible to use the signal obtained from the strain on the surface of a given component to which it is attached, and convert it in an electrical signal proportional to the applied load. The electric strain gauges are the sensors which are normally bonded to the surface of a metal alloy cell to produce the electric signal. The use of electric strain gage relies on the variation of the ohmic resistance, whereas the deformation occurs. Figure 17 shows some examples of strain gages commonly used in the construction of load cells.

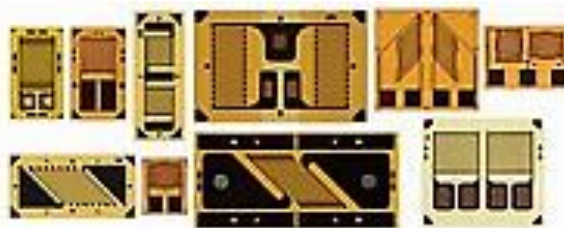


Figure 17. Strain gages [24].

In order to obtain an electrical signal that can later be recorded and processed on any computer, it is necessary to convert the ohmic resistance variation into an electric voltage, which can then be converted into a digital signal. The electronic circuit normally used for this purpose is the Wheatstone Bridge, that can be seen in Figure 18. This circuit includes four branches where one or more electric resistances can be replaced by strain gages. With the Wheatstone bridge is possible to assess small electric resistance variations and allows to reduce the associated errors, raising the reliability of the signal measured. The imbalance of the circuit's power supply, due to the strain gages deformation and its implicit resistance variation, is proportional to the magnitude of the force applied.

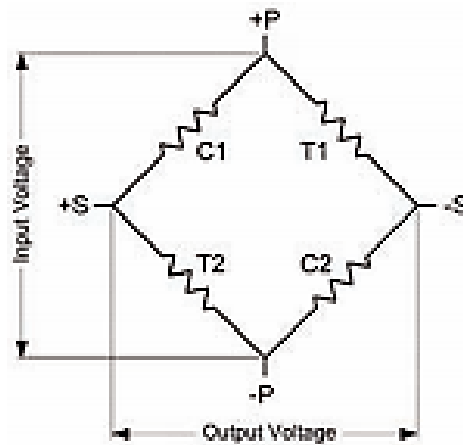


Figure 18. Wheatstone bridge scheme [24].

As a minimal amplitude variation can lead to a high related error, and the proportional ratio should be kept, the sensor is a fragile and complex instrument. The Circuit Bridge endures a correction to the possible temperature-caused hysteresis; also, creep and repeatability phenomena are considered [24]. This solution is often used in structural engineering to yield structures or component strain, especially when their safety is mandatory and it is necessary to early anticipate situations of damage or failure.

## 2.5. State of the Art

The human skeleton supports the loads applied on the body, whether resulting from the action of weight or from locomotion or even from physical activity. When a bone fracture arises the skeleton reduces its load bearing capacities so it needs a healing process that restores its functions. If fractures occur in the longer bones, it is mandatory to immobilize the fractured parts and restore the ability to support load. The cure time depends on several variables, either intrinsic to the individual or resulting from the biomechanics that the immobilization process implies.

The concern to monitor bone healing and regeneration in fracture remains visible in several biomechanical fields. Since the middle of the last century, many techniques have been used to describe behaviour and quantify biological and mechanical variables to ensure the best treatment for a serviceable and effective recovery. In this segment, it will be referred some

articles that adopt different techniques to fulfil this purpose, corroborating the imminent importance to its success.

### 2.5.1. Using Percussion Signals

Many attempted to assess the extent of the healing process using bone percussion notes. In a study conducted by Sekiguchi et al., they found that percussion waves, caused by a vibratory stimulus in the bone, should be analysed periodically, and the evolution of its graph should tend to the assimilated characteristic in an intact evaluated bone [25].

Many attempts were made between 1932 and 1967 to make this technique feasible and a reliable criterion for health professionals. Given the failure of these studies, a new approach was concerted: the measurement setup consists of a tapper, mechanically maneuvered and using an elastic spring with known properties, which produces a consistent vibratory stimulus in the medial malleolus; and a signal collection device located in the tibial tuberosity's medial region, which includes a pick-up, a 10Hz-100KHz frequency band transistorized amplifier and a data display [25]. From the application of the experimental protocol to a bone in consolidation process and an intact bone, some interesting facts emerged:

- it has been concluded that the percussion signal of an intact bone is characterized by an almost constant pattern along the vibratory stimulus, and, in fact, bone consolidation progresses to equalize these attributes [25];

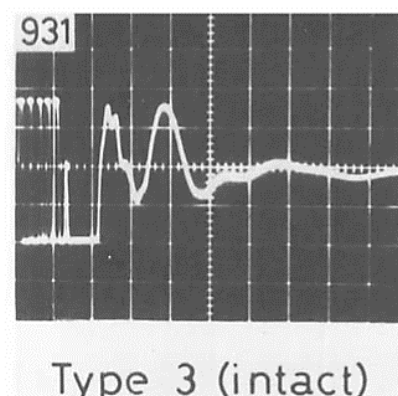


Figure 19. Intact bone p-note [25].

- In the analysis of the frequency spectrum, a great difference between the percussion waves of the intact and fractured bones was evident, around 700Hz-4800Hz, concluding that

there is a great attenuation at high frequencies in the fractured bone's graph [25]; this conclusion follows the behaviour of the structures because, for the same mass, the higher vibration frequencies correspond to structures with greater stiffness.

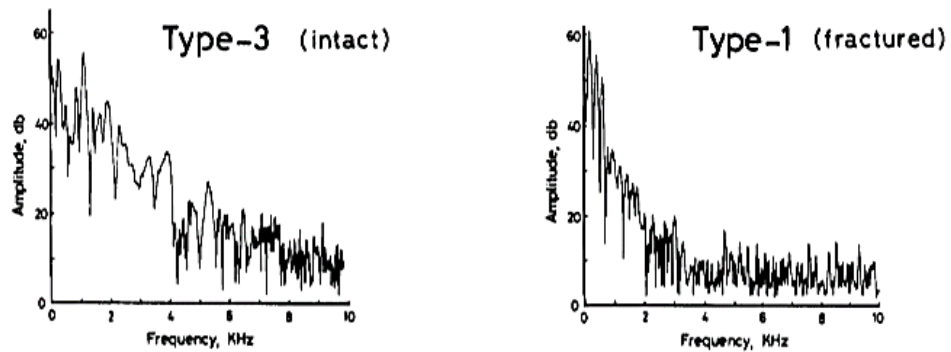


Figure 20. P-note's frequency spectrums [25].

- From the temporal observation of the percussion note, it is understood that, as consolidation is established, the notorious cycles in the measured wave are increased, going from an initial type 1 phase, with only 1 evident period, to type 3, which presents several perceptible wave cycles [25];

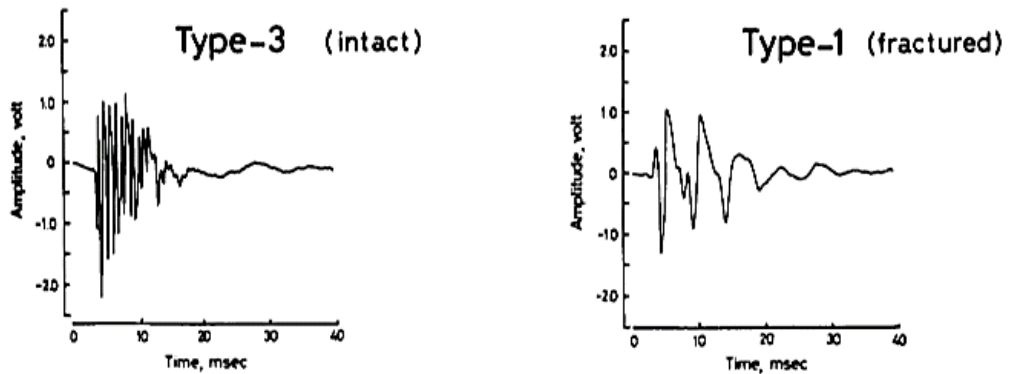


Figure 21. P-note's temporal Spectrums [25].

- It was also decided to establish a mean time of normalization of patients submitted to this process from 2 months to 1 year, according to the initial state of consolidation at the beginning of the tests. In this way it becomes possible to monitor the bone healing process, following its patient evolution and fracture type using the dynamic response to a load impulse [25].



### 2.5.2. Measuring Bending Stiffness

In a study conducted by *Hente et Al.*[26] they attempted to develop a device that would measure, as rigorously as possible, the bending stiffness of the bone, even under conditions in which external fixator's pin was not fully tightened. These biomechanical properties can be quantified to deduce the behaviour and state of the bone consolidation at each stage of recovery [26].

The method they comprised, and tested in vivo on sheep's tibias, consisted of an adapted aluminium fixator, which was proved at a 4-point bending regime. For this, a load cell was coupled to the external fixator system, allowing the application of a force, approaching or separating instrument's clamps, causing a flexion effect in the bone. The results were obtained by drawing the graph that represents the relation between load and deformation in the corresponding bone system [26].

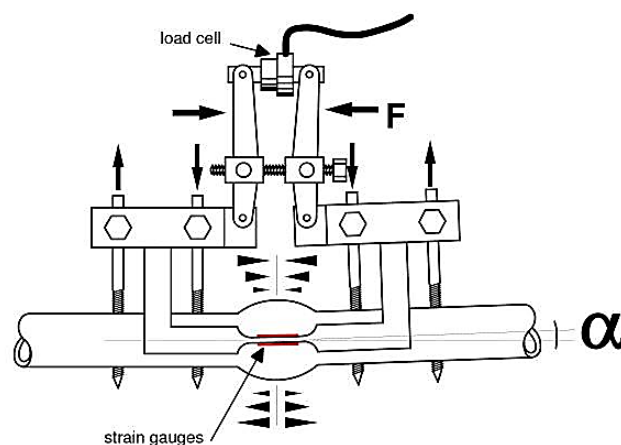


Figure 22. Bending stiffness measurement apparatus [26].

The measuring device requires a calibration using aluminium bone models, and simulating various bending fractures, as well as several degrees of Pin Loosening. All the parameters were considered to draw the calibration line that allowed to define the relation between load and angular deformation. The more accentuated the slope of this relational curve, the lower the stiffness modulus of the material under test [26].

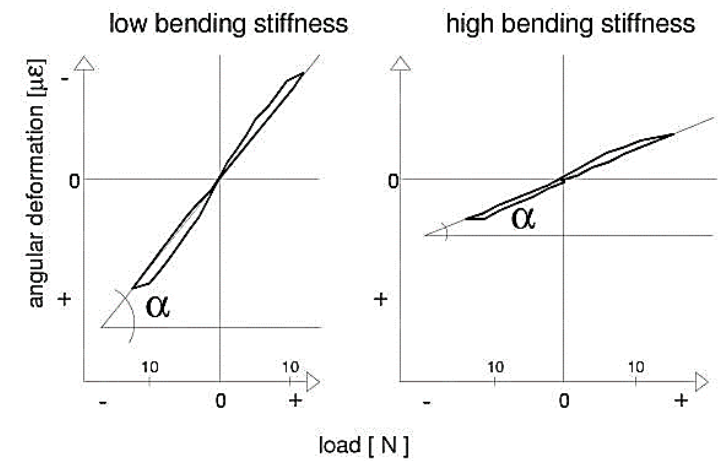


Figure 23. Load-Deformation relation [26].

Starting on the evaluation of patients undergoing this treatment, it was concluded that Pin Loosening is a recurrent problem, occurring in 75% of the evaluated cases. Thus, the evaluation of the flexion stiffness allowed, not only to evaluate the good evolution of the bone consolidation process, but also to assure the point at which it is possible to remove the fixator, avoiding the occurrence of Pin Loosening phenomenon, and not affecting total and effective patient's recovery. That threshold point is at 15 Nm/degree for human tibia, with an 3,4% error when one pin is loosened, and 29,3% when there is a loss of constriction in 4 pins [26].

The study allowed to go further and to establish a predictive model of the bone consolidation behaviour: it was possible to find a logarithmic relationship between bending stiffness after 3/4 weeks and stiffness after 7/10 weeks [26].

### 2.5.3. Using Ultrasonic Waves

Electromagnetic fields have direct biological effects in endochondral cells and on the formation of bone callus, actively contributing to the acceleration of the healing process when subjected to an injury. Using this proven assumption, researchers at the Greed University of Ioannina have created a wearable device that uses ultrasound signals to monitor and accelerate the process of bone callus consolidation and maturation. This device also makes it possible to maximize the accuracy of information related with the healing process and to recognize possible problems at an early stage [27].

This apparatus consisted on a system that was coupled to an external fixator, with two transducers dermally-placed in both fracture's epiphyses, being used to transmit ultrasonic waves through the injured site. The system includes a whole data collection and treatment process, being the signal rectified, filtered and selected, in addition to the inherent data extraction. It is possible to access information at any time, allowing a temporal evaluation of osteogenesis [27].

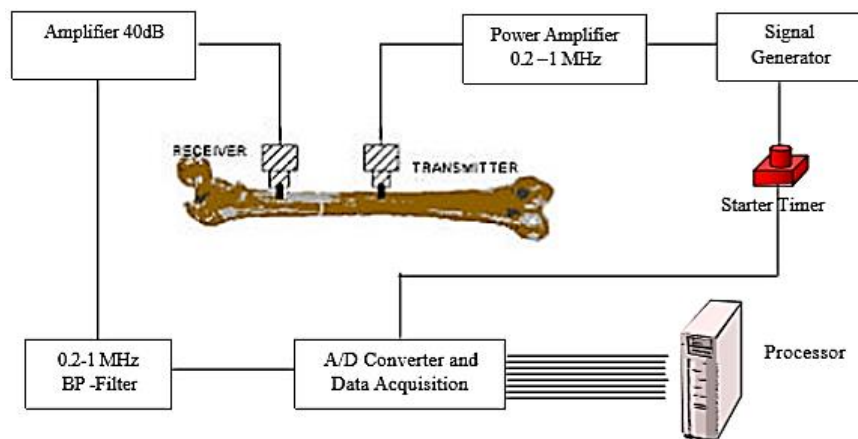


Figure 24. System's architecture [27].

The evaluation of callus maturation is possible by the determination of two variables, namely Ultrasonic wave propagation velocity and Distortion spectrum. The first variable dictates that velocity is associated with bone elasticity and density: as the callus has different properties compared to the bone, the velocity in this zone will be inferior to the standard speed; in other hand, distortion of the obtained signal is associated with changes in the architectural microstructure of the bone to be repaired [27].

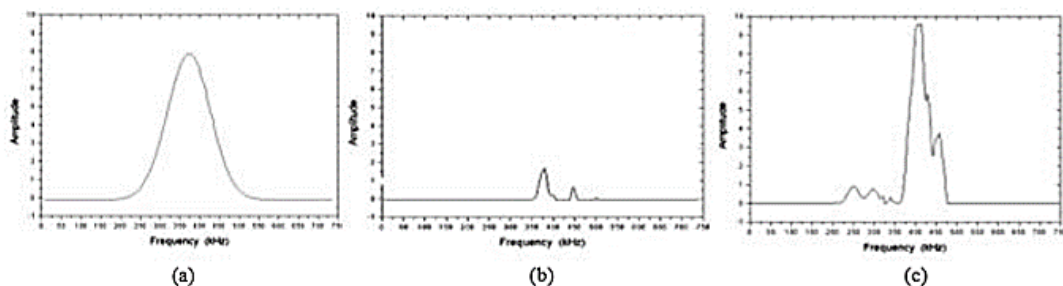


Figure 25. (a) Transmitted signal, (b) signal received, after surgery, (c) signal received, during consolidation [27].

#### 2.5.4. Load Cell Transfer Function

It is also possible to describe the state of union of a fractured bone from the dynamic response to a set of pulses of about 200-600 Hz. Using the assumption that vibratory response of a bone is directly associated with its state of consolidation, the discrete impulse response can be analysed to evaluate progress. In this case, the sensitive element need to be dermally-located, and may act without significant interference on one of the outer pins of the external fixator, not interfering with the construction of the immobilization device. This device was not allowed to quantify the stiffness associated to the analysed bone, being therefore a complementary technique [28].

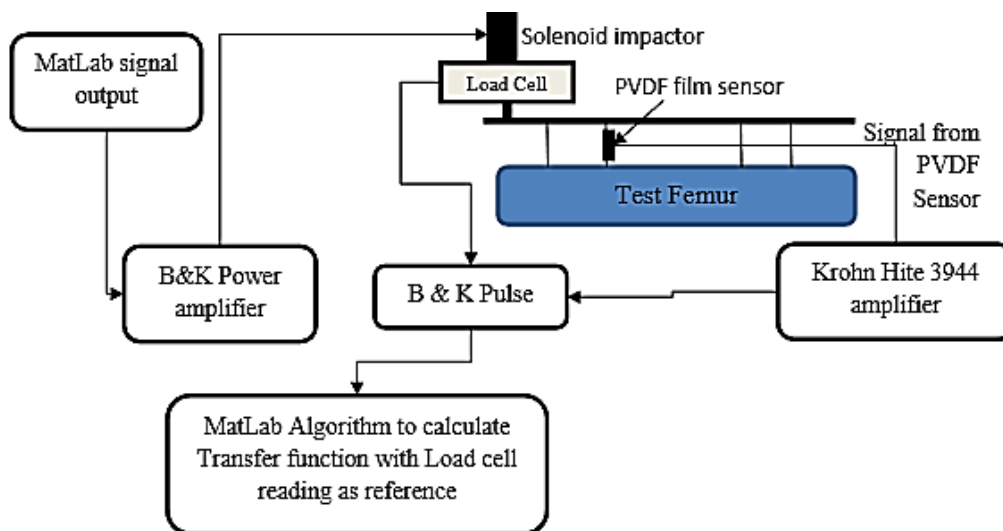


Figure 26. System's architecture [28].

# Chapter 3. Biomechanics of the Tibia

## 3.1. Biomechanical Principles

Human skeleton is subjected to a set of forces, either it is in a dynamic or static condition. Static conditions are basically reduced to gravitational forces associated with body's weight; when in a dynamic behaviour, the previously referred gravitational forces are amplified in magnitude and occur in different directions. These features are concordant with the support and movement functions of the skeleton [29].

Bones are routinely subjected to two types of forces, internal and external forces. The internal forces, associated to the postural and movement conditions of the body, are transmitted through the joints and tendons. The external forces present no limitation of magnitude and unpredictable orientation, being able to cause bone fractures. The force's magnitude and orientation, adding to the bone's geometry and composition, dictate the degree of deformation of the bone. The applied force produces a load in the affected structure, that can be materialized into several types of loading. If the magnitude, allied to its direction, overcome the bone's resistance limit, occurs a fracture which can occur for different loading conditions as represented in Figure 27. [30]

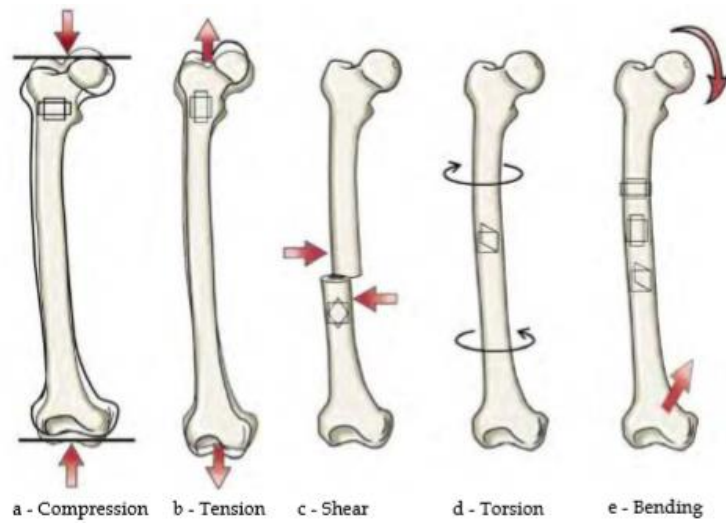


Figure 27. Types of loading that a long bone is subjected [31].

When a structure is subjected to a load, it is produced a set of deformations. Those deformations are a function of the constitutive properties and structure geometry, so it can be inferred that different materials produce different responses to an applied load. In order to characterize a material by its stiffness, the determined quantities must be independent of the geometry of the structure. This is accomplished through a structural diagram, that relates the stresses induced with the strain caused. The normal Stress,  $\sigma$ , is defined as the Load,  $F$ , divided by the section where it is applied (Equation 3.1). The SI unit of the Stress is the Pascal (Pa), being equivalent to Newton/squared meter ( $\text{N}/\text{m}^2$ ).

$$\sigma = \frac{F}{A} \quad (3.1)$$

Strain,  $\epsilon$ , represents the change in dimension of a body under the action of a force or multiple forces, as can be seen in Figure 28. As natural, a normal Strain is caused by a normal Stress, and it is a measured of the modifications in length,  $L$  (Equation 3.2).

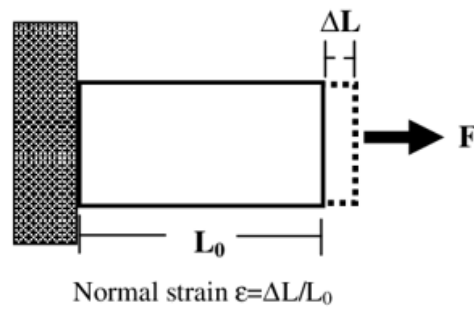


Figure 28. Strain scheme [32] .

$$\varepsilon = \frac{\Delta L}{L} \quad (3.2)$$

The slope of the linear/elastic part of the graphic representation of the Stress-Strain plot, inherent to the given material, is intended as the Young's modulus (E):

$$E = \frac{\sigma}{\varepsilon} \quad (3.3)$$

The Young's Modulus has units similar to the Stress, Pa, since the Strain is an adimensional variable, and it is a characteristic of the constitutive material, independently on the geometry presented.

The bone is a viscoelastic and anisotropic material; is capable of supporting compressive loads and presenting some pliability on a tensile regime, varying its behaviour depending on the force orientation. Depending on the bone type, the inherent mechanical properties, reproduced by the stress-strain curve, differ as can be seen in Figure 29 [29]. The referred image represents a typical scheme of the stress-strain curve, for each bone type.

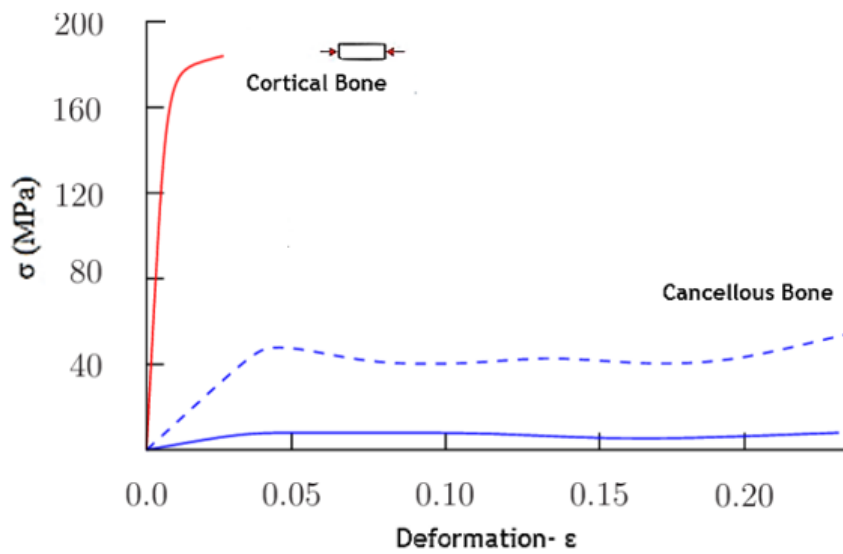


Figure 29. Typical Stress-strain curve for cortical and cancellous bones (adapted from [33]).

The cortical bone's higher mineralization makes it stronger and stiffer, but it lowers the toughness: it means that the bone can support a bigger load until fracture, while the plastic region where deformation occurs is feeble. That is the reason why cortical bone is usually found in the shaft of long bones and as a shell around cancellous bone. The cancellous bone, being a porous structure, is less strong, but highly conducive to deformation until fractures. Differing from the cortical bone, the plastic region in this material is extensive [30][29].



## Chapter 4. Finite Element Modelling

The Finite Element Model (FEM) is the numeric tool frequently used for the analysis of osseous architectures in structural mechanics. When a structure is loaded, tensions are generated in its constituent materials, characterized by their magnitude and orientation, and, as a whole, by their distribution along the structure's volume [34]. Those attributes depend not only on the constituent materials' properties and their spatial and geometric organization, but also on the intensity and position of the applied loads, and the system's boundary conditions [35].

The FEM allows to divide a complex problem into several simpler ones through discretization of the global structure. It uses a system of points, named as nodes, which form a mesh. The possibly intricate structure of the problem is thus divided into a finite number of regular geometry blocks, its elements, which connect in specific locations with the nodes, in a geometry with facilitated analysis compared to the initial one.

In the biomechanics field, the FEM has been an important asset, allowing the analysis of complex states of stress and deformation that are arduous to determine in *in vivo* experimentations. Furthermore, it allows to provide the distribution of deformations and stresses in the analysed geometry, predicting the occurrence of fractures or ruptures at a specific location, or evaluating the behaviour of a certain implanted device.

### 4.1. Finite Element Method Evolution

The FEM began to be developed in the 1950s in the aerospace industry and it was later introduced into orthopaedic biomechanics in 1972. In that epoch, it was used to assess stresses in human bones and to optimize implants and its fixation techniques. In 1960s, *E. Wilson* [36] developed one of the first finite element programs, although this was only limited to two-dimensional stress analysis. The referred program has proved its usefulness and several academic research groups and industrial laboratories have finally used and upgraded it. In 1965,

NASA funded a project led by Dick MacNeal [37] to develop a general application finite element program, originating “NASTRAN”. This software was the first capable of run three-dimensional analysis in a wide variety of applications. This was the starting point for the development of several finite element programs: in 1978 was funded the company that would found ABAQUS®, the most used software in academic environment [35].

## 4.2. 3D Modelling of the Tibia

For the attainment of the finite element three-dimensional model it was necessary to have an idea about the Tibia’s anatomy. That research can be previously seen in the section 2.1. The construction of the model will be subdivided in five main components: cortical bone, trabecular bone, medullary canal, osseous callus and the external fixator. In this chapter will be presented the methodology for the achievement of the tibia model.

### 4.2.1. Obtainment of the three-dimensional geometry

The first step in the creation of a finite element model is to represent the tibia geometry in the computer. Using some medical imaging techniques to make an image faithful to reality, it consists on a sketch of the superficial topology of the left tibia: the model is just a monolithic and compact cortical bone’s construction with an appearance similar to a regular tibia. The model is distributed by Sawbones®.

A 3D model of the left tibia was achieved using a Computed Tomography (CT) based technique. CT is an x-ray imaging procedure capable of producing signals that are processed and translated to generate bi-dimensional cross-sectional images of the body. These images are equally spaced between them forming a set of slices that, when stacked together, form a three-dimensional image of the analysed body.

All geometries were created using a computer-aided design software, SolidWorks®. The intended final model of the tibia part is composed by a three-layered body that could be compared to the main structure of a lower limb bone. Besides the cortical bone layer, it will be take into account the trabecular osseous sheet and the bone marrow located centrally. The considered tibia 3D model is represented in figure 30.



Figure 30. Tibia 3D model: posterior(a) and anterior(b) views.

The dimensions of the tibia were obtained from Solidworks®, and are reported in Figure 31. The bone has not a perfectly round section in the middle, instead it presents an oval form, justifying both diameters referred as the ellipse axis.

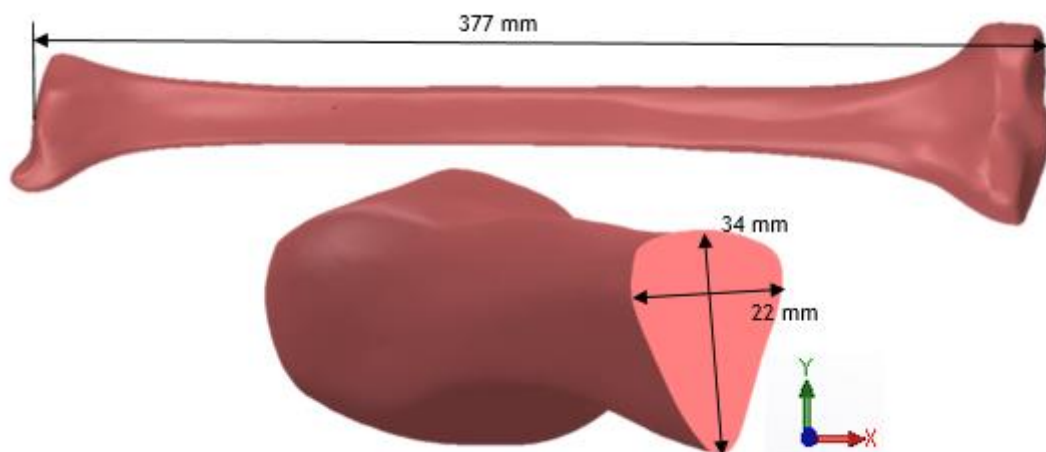


Figure 31. Tibia model dimensions.

Firstly, it was created a compact and sized body that resembles the trabecular bone' external geometry. The topology of the trabecular bone is approximate to the cortical bone's, merely differs on a subjective fillet on the epiphysis, so it can be built through a non-uniform scalar diminution of the first stage model. To achieve the correct spatial coordinates to scale the model is mandatory to balance the physiological requirements and the interference conditions in the model. In a study conducted by Arjmand et Al. [38], they found that the

cortical bone has a thickness of approximately 2.5 mm along the proximal epiphysis; that metrics will be intended for both the epiphysis and diaphysis.

After the creation of a solid model representing the trabecular osseous layer, the model needs to be hollow. In this phase it remains two bodies: the final arrangement of the cortical bone and a primary solid model of the trabecular bone.

In order to insert internally the canal with bone marrow, a cylinder with 8mm diameter was created, reasoned by the metrics of the physical bone model used in second stage, what simplifies all the process of construction and hollow [39],

The intricate concern lasts with the location of the canal, located not exactly in the arithmetic centre of the tibia plateau [40]. The inferior view of the tibia distal region, a constituent of the tibiotarsal articulation, announce the canal position, which is concordant with the stipulated by *Sang Jun Song et Al* [40]. The mentioned protuberance can be seen in Figure 32 through a salient circumference in the surface.

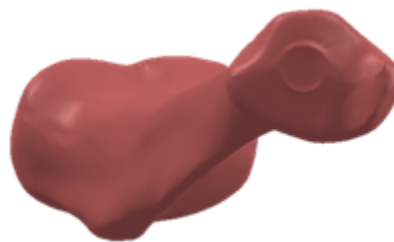


*Figure 32. Distal Epiphysis' inferior view.*

Thereby, the medullary cavity is located in a posterolateral region compared with the surface arithmetic centre. After positioning of the canal the tibia model was obtained, as shown in Figure 33.

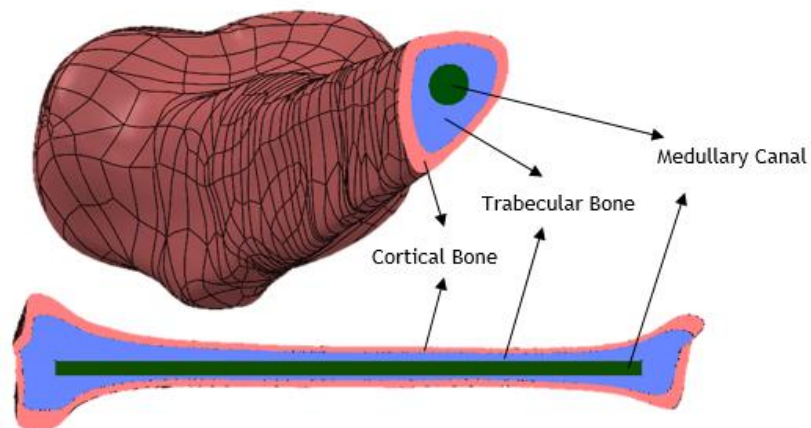


Figure 33. Tibial model sections.

After the tibia model completed, it was created two kinds of fractures: an oblique fracture and a transversal one, Figure 34 (a) and (c), respectively. A fracture gap of 3mm was created in the middle of tibia's longitudinal axis. In case of the oblique fracture an angulation of  $30^\circ$  degrees was considered. The geometry of the callus was generated in the fracture gap and modelled with a structure similar to the section of the bone, but passable to own callus-like properties. Tibia models with callus are presented in Figure 34 (b) and (d).

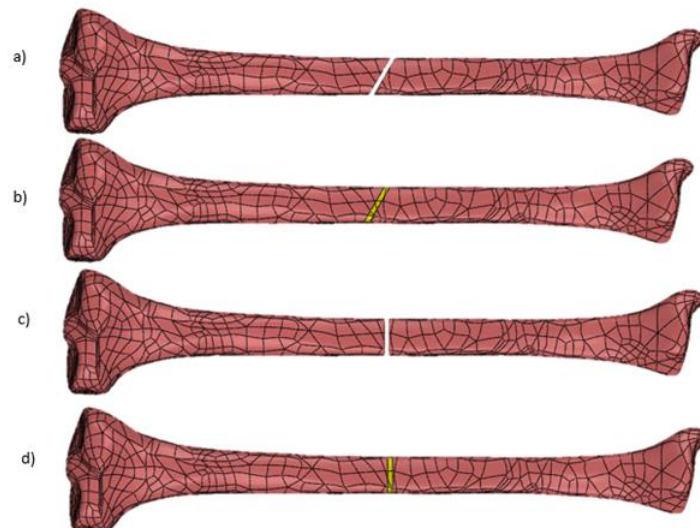


Figure 34. a) Tibia with  $30^\circ$  fracture b)  $30^\circ$  fracture with callus c) Tibia with transversal fracture and d) transversal fracture with callus.

After the two 3D models of the fractured tibia were built, it was necessary to create an apparatus that could mimic the functioning effect that a fixator has in the treatment process. That could be achieved using a simplified fixator implemented directly in the tibia, through a set of six well-spaced and located cylindrical pins, and a cylindrical rod perpendicular to them that ensures their connection and positioning. The fixator set is perfectly symmetrical relatively to the plan that divides the callus in half. The fixator model was based in the Hoffman 3 External Fixation System of Stryker®, what dictates the dimensions of pins and rods and their location [41]. The dimensions of the components of the fixator are provided by the manufacturers and summarized in Table 2.

*Table 2. Dimensions of components of the fixator model (based in the Hoffman 3 external fixator)[41].*

<b>Fixator's components</b>	<b>Dimension (cm)</b>
<b>Pin Length</b>	12
<b>Pin diameter</b>	0.4
<b>Rod length</b>	36
<b>Rod diameter</b>	2
<b>Distance between Pins</b>	2.3
<b>Distance from central pins to the callus middle axis</b>	7

Two aluminium supports were created in both 3D models that is being used for the experimental tests, allowing the tibial fixation and linear orientation. It consists of two parallelepipeds with equal section area located in the distal and proximal extremities of the tibia. The final models can be seen in Figure 35.

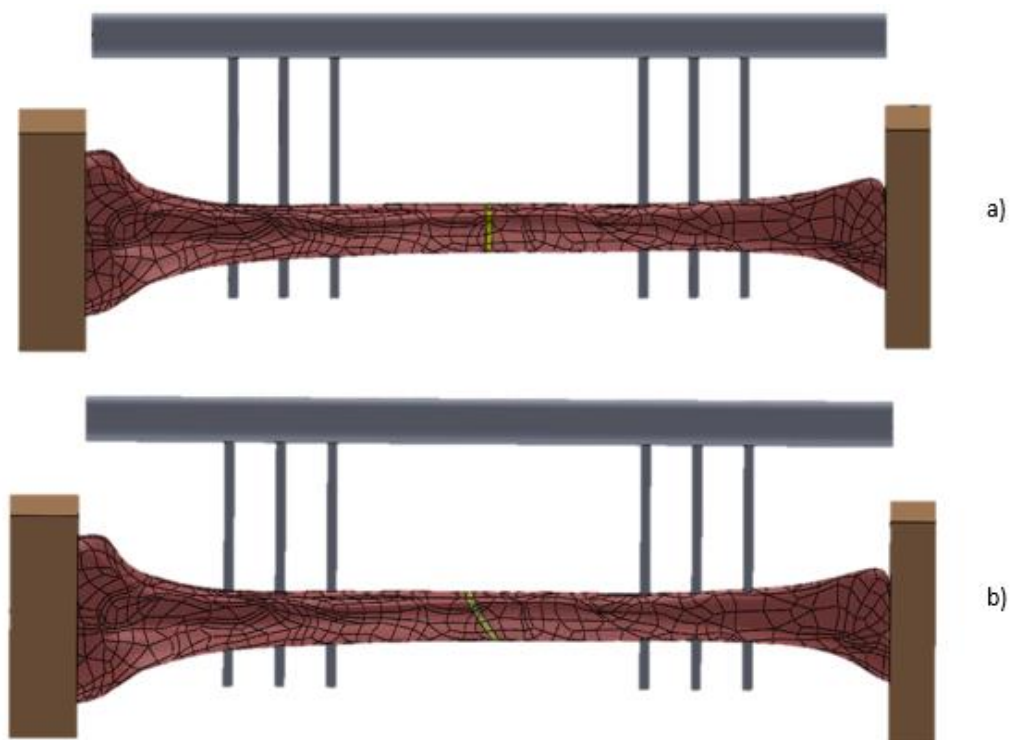


Figure 35. Model of the fixated tibia with transverse fracture (a) and oblique fracture (b).

#### 4.2.2. Finite Element Mesh

After the acquisition of the tibia's geometry, the model is imported to a software able to perform finite element analysis and computer-aided engineering, in this case ABAQUS®. All the surfaces were meshed in order to sharp a better resolution model. Using the existing automatic meshing tool from the software, it is created a mesh, part by part, based in a given geometry figure with defined size. In the framing of a finite element mesh, the selection of the finite element geometry must take into account the complex shape of the model, in order to adjust to its contour.

The cortical bone, represented in Figure 36(a), has a mesh based in a quadratic tetrahedral element C3D10 and a number of 165665 elements and 264007 nodes. That was performed using an automatic global size of 2 units.

The mesh of the trabecular bone, that can be seen in Figure 36(b), has exactly the same geometric and refinement degree properties of the cortical bone, but its lower global surface area presents 131973 quadratic elements and 198382 nodes.

The medullary canal presents a more regular surface than the bone, so in this case, it was used a linear hexahedral element as the base for the meshing. That structure has 4150 nodes through all its 2970 elements. The final geometric mesh can be seen in Figure 36(c).



*Figure 36. Tibia's components mesh.*

Beyond the 3 main components of a normal tibia, a fracture was inserted and filled with a callus complementary to the original model. The callus was also meshed in the Abaqus® software according to the same parameters used in the osseous materials. Thereby, it was generated a quadratic tetrahedral element based mesh with 3735 nodes and 2125 elements. The referred structure can be seen in Figure 37.

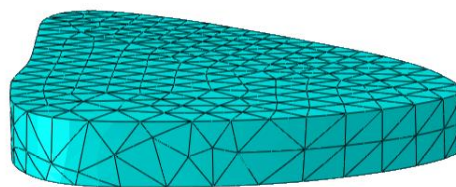


*Figure 37. Callus mesh.*

To ensure the fixation of the fractured tibia, it is also necessary to simulate the external fixation approximated device. To fulfil the most reliable results, the degree of refinement of the fixator must be adapted to the tibia one. Basing on that statement, a quadratic tetrahedral



element C3D10 was used as a monomer for each mesh. A set of 124738 nodes and 85000 elements was used in the cylindrical rod mesh, while each pin has 3621 nodes along its 1888 elements. The instance intended as the fixator has its mesh shown in Figure 38.



Figure 38. External Fixator mesh, constituted by a rod (a) and pins (b).

The epiphyseal frames, represented in Figure 39, also endues a C3D10 tetrahedral based mesh. The proximal epiphysis frame (a) has 270224 nodes between its 190221 elements. The frame located distally possess 125914 elements and 180388 nodes.

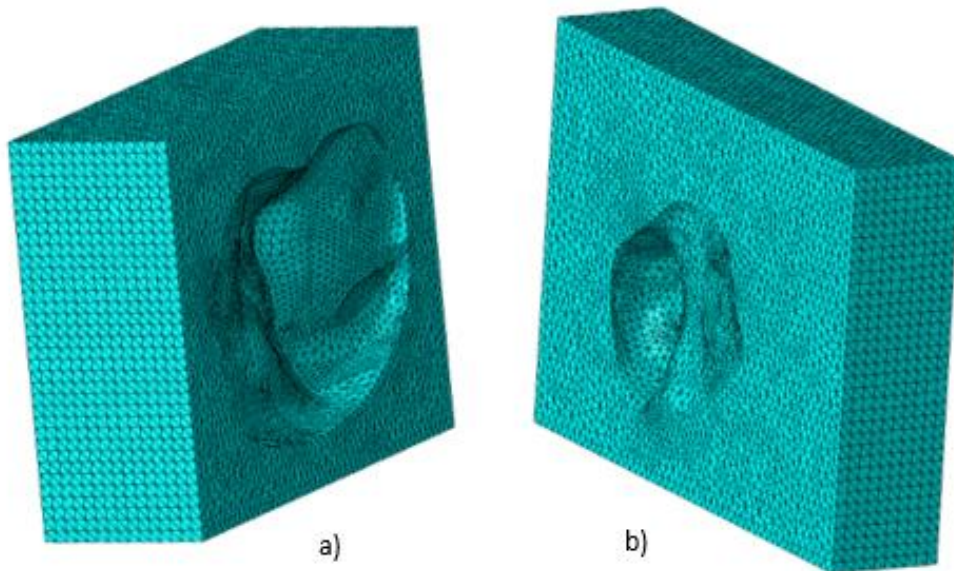


Figure 39. Proximal (a) and Distal (b) frames' mesh.

### 4.2.3. Constitutive Model and its mechanical properties

The selection of the constitutive model must take into account the particularities and the purpose of the study, as well as the interactions between the components and its significance for the final model.

The medullary cavity, that fills the inner layer of the bone, was intended like a soft tissue, in detriment of its fluid component [42]. Those assumption lasts with the surface interaction with the inner surface of trabecular bone, inferring a viscoelastic behaviour to the structure.

Similarly, the behaviour of the cortical bone was simplified in order to fulfil the requirements of the model. Normally, when applied a load in the bone, its longitudinal direction is capable of bearing a higher amount of load than any of its perpendicular directions [31]. The mentioned fact proves the anisotropy inherent to the cortical bone. In this case, the load is assumed perfectly vertical, being parallel to the longitudinal axis of the model: thereby, assuming a mechanical behaviour solely with the longitudinal direction contribution, the model can be simplified and the cortical bone assumed isotropic [43].

Each component of the tibia and the external fixator was defined in term of its mechanical properties: Young's modulus, Poisson's ratio and density. All materials were assumed to be homogeneous, isotropic and linearly elastic. The values used for cortical bone, trabecular bone, medullary canal, rod and pins are reported in Table 3.

*Table 3. Mechanical properties of tibia and components of external fixator.*

<b>Material</b>	<b>Young's modulus (MPa)</b>	<b>Poisson's ratio</b>	<b>Density (Kg/m<sup>3</sup>)</b>	<b>Reference</b>
<b>Cortical Bone</b>	16700	0.3	1640	[43]
<b>Trabecular Bone</b>	1100	0.3	200	[43][44]
<b>Medullary Canal</b>	1	0.167	-	[45]
<b>Aluminium (Rod and frames)</b>	69600	0.33	-	[46]
<b>Steel (Pins)</b>	211000	0.29	-	[47]

The callus was simulated considering different mechanical properties. The intention is to have the representative behaviour of each healing stage, in a range of elasticity values that vary between the initial soft callus, until a phase that represents the hard callus stage [45]. All the different phases properties are described in Table 4.

*Table 4. Callus properties in the various stages[45]*

	<b>Young's Modulus (MPa)</b>	<b>Poisson's ratio</b>
<b>Fibrous Tissue</b>	0.2 - 5	0.167
<b>Cartilage</b>	5 - 500	0.167
<b>Immature bone</b>	500 - 1000	0.3
<b>Intermediate bone</b>	1000 - 2000	0.3
<b>Mature bone</b>	2000 - 6000	0.3

#### 4.2.4 - Load and Boundary Conditions

After the construct of the mesh, it was decided the simulation conditions that makes possible the mechanical analysis of the model. The selected conditions intent to mimic the circumstances that the tibia is subjected on a given state.

In a static state, it is normal to assume that the muscles forces do not affect the global resultant force, being only cincture to the body weight [48]. For an average body weight of 80 Kg, a compressive load of 800 N was applied on the upper surface of the proximal extremity. That force causes a uniform pressure in the superior surface of the proximal epiphysis of the tibia. Despite the global force is usually biomechanically divided into the two lower limbs, it is intentional to subject the referred tibia to that pressure, denoting disparities all along the bone.

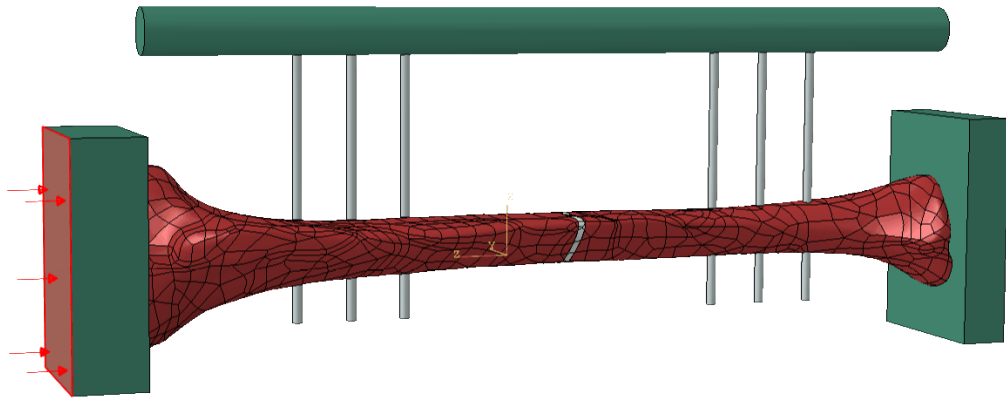


Figure 40. Load applied in the transverse fractured bone model.

The distal extremity, constituent of the tibiotarsal articulation, was fixed, with no displacement or rotation allowed in any direction [48], as can be seen in Figure 41. As a consequence of the knee joint in the proximal region, all the lateral surfaces of the proximal base, correspondent to the proximal epiphysis were fixed, with no rotation allowed in lateral directions. It can be seen in Figure 41.

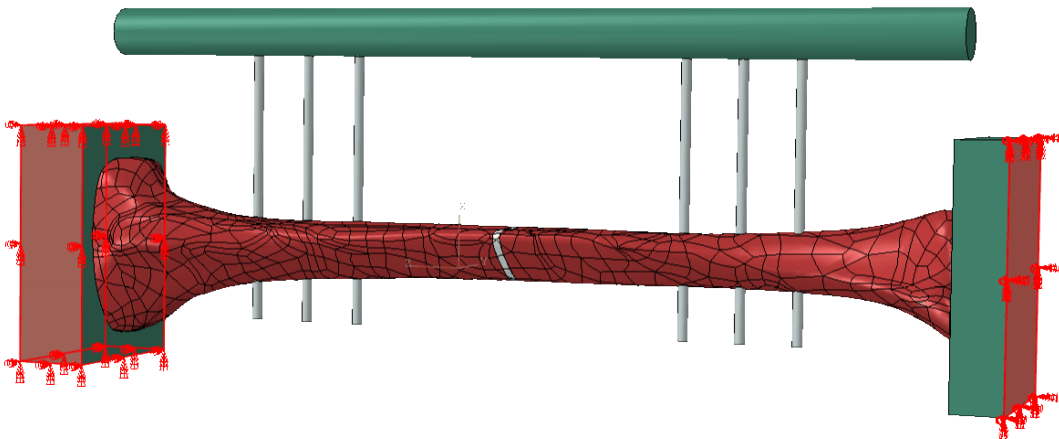


Figure 41. Boundary conditions in proximal and distal regions of the transverse fractured bone model.

## Chapter 5. Experimental Tests

In this chapter, it is presented all the methodology adopted for the performance of mechanical tests in a synthetic bone coupled to an external fixator. The bone structure was subjected to a 3 mm transversal diaphysary fracture, that will be filled with discs whose intention is to simulate the regeneration callus. The discs are composed by several materials, with different mechanical properties, that intent to represent each phase of bone consolidation process. Therefore, after characterization of each sample and possible attribution to a given callus phase, it would be possible to predict the callus' behaviour when subjected to a defined force.


### 5.1. Samples Characterization

#### 5.1.1. Materials used

To characterize the different phases of healing, it was selected some materials that could be manipulated to obtain different rigidity levels. Therefore, the presumptive path was to choose a mixture of materials that, when added in several ratios, acquired different properties. Due to that requirement, and its ease access, it was selected an Altropol rubber, an epoxy resin and a silicon.

Altropol rubbers outcome from the mix of two components and a hardener material. The addition of different quantities of each one of the three components results in sample with distinct mechanical properties. The ratios used can be seen in Table 5.

Table 5. Altropol rubber samples [49].

Components	Ratio of Components	
NEUKADUR ProtoFlex 150-05	100	90
NEUKADUR ProtoFlex 190-05	0	10
Hardener PTG 1	20	23
Altropol rubber samples		

The epoxy resin (Figure 42(a)) was also obtained through a mixture of two Sicomin components: SR1500 resin and SD2505 hardener, in a proportion of 100:33 [50]. If the proportion were not integrally fulfilled, the risk of the resin not cure is quite high. The silicon rubber was obtained by a bicomponent mixture named HT 33 transparent. The final product is a equiproportional junction of a base and a catalyst that vulcanizes at room temperature [51]. The silicon specimen can be seen in Figure 42(b).

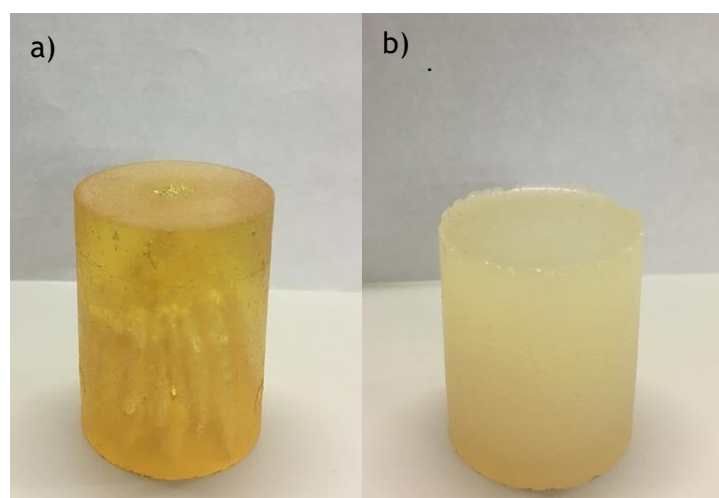


Figure 42. Epoxy Resin (a) and Silicon (b) samples.

The last material was reused from a former experiment done in the department. The integrity of the product was ensured what made viable the recycling of the substance to create a sample worth to be used. The sample is also a bicomponent of an epoxy resin and a hardener, whose ratio is unknown. This sample will, from now on, intended as the “Gray sample” (Figure 43).



*Figure 43. The Gray sample.*

### 5.1.2. Materials characterization test

All the previously mentioned mixtures were molded into a shape that facilitates its posterior insertion in the fracture gap of the bone with external fixator. Thereby, it was created a Teflon mold with a defined cylindrical form, that can be seen in Figure 44. The cylindrical shape mold has the cross section whose geometry is the most similar to the fracture one, being the obvious selection in terms of geometry. The materials choice is due to Teflon's high temperature tolerance, in case a cure is needed, and its non-reaction with the chosen materials [52]. All the samples dimensions follow the indicated norm ASTM 1621-00 which provides guidelines for Compressive Properties of Rigid Cellular Plastics [53].

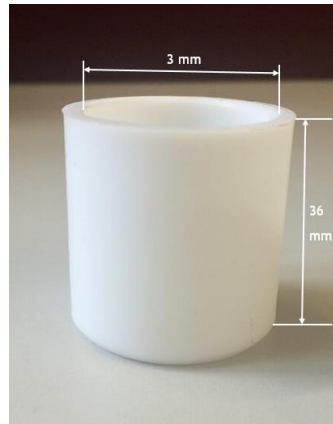


*Figure 44. Cylindrical shape mold.*

The mechanical tests for the samples' characterization were executed in a dynamic and static compression test instrument, located in LOME, named Instron EletroPuls E1000 [54]. In datasheet of the Instron E1000, this machine has a dynamic and static load capacity of 1000N and 710N, respectively.

All the compression tests were performed at a crosshead speed of 2.5 mm/ min, using a preloaded on 50 N that allows the correct insertion and positioning of the sample, and a maximum threshold of 1000 N. The Instron E1000 and some compression tests can be seen in Figure 45.



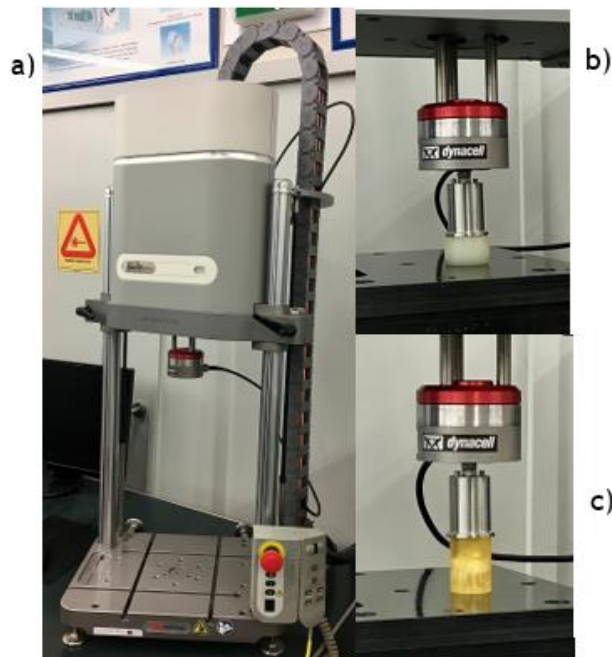


Figure 45. (a) Instron EletroPuls E1000. (b) Compression test executed for the characterization of the Silicon sample. (c) Compression of the Epoxy Resin sample.

After the performance of the test to all five samples, the output is a series of values that relates the force applied in each instant to the displacement in the specimen. The characterization of a material is accomplished by its Young's modulus, that is numerically equal to the slope of the characteristic Stress-strain curve of a given material. With the acknowledgement of Equations 3.1, 3.2 and 3.3, it is possible to manipulate the obtained file of values to a set of variables that allow the tracing of the pretended graph.

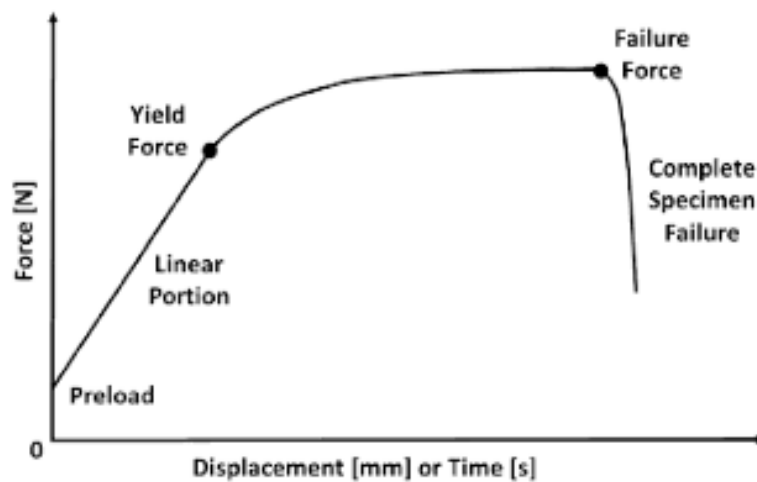


Figure 46. Force-displacement curve of cortical bone [55].

### 5.1.3. Samples' characterization results

After the values' manipulation, mentioned in the previous subchapter, it was possible to obtain the Young's modulus. All the samples were tested until the same level of force, and none of them reached a rupture stage. It is also important to refer that all the samples have the same cross-section area, but different heights, factor that was taken into account in the analysis of strain. In Figure 47 is represented the stress- strain curve for the samples under test.

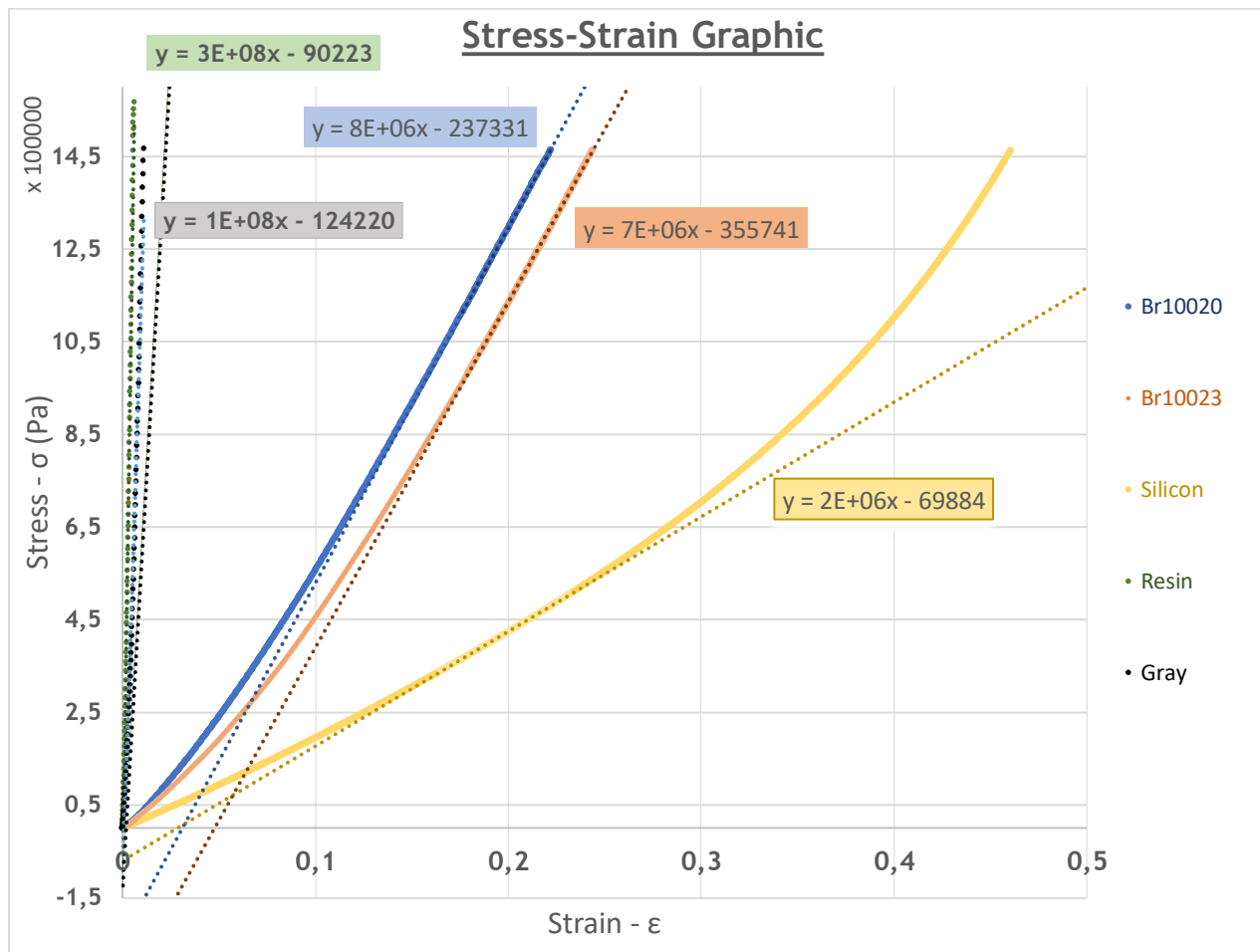


Figure 47. Stress-strain curve for the samples under test.

Analysing the stress-strain curve of all materials to the test, the results indicates that the silicon material presents the smaller Young's modulus (2 MPa) The physical comprehension of that statement foresees that if applied a certain limited force to every samples, the silicon will present a bigger amount of deformation.

Following the same logic, the results shown that the resin material is the most rigid one. The previous statement is holded by observation of the graphic, where is possible to noticed that the resin has the biggest slope among the materials presented. According to the calculations, the value of the Young's modulus was 300 MPa.

In the analysis of the Altropol-based samples, it is perceived a discrepancy: in a pre-test analysis it is expected that the sample with high quantity of hardener will present highest stiffness [49], and that does not occur. The results showed that the sample with a ratio of 100:20 presents a higher elasticity modulus than the 100:23 sample. The results may have been influenced by a defective components' measurement or unsatisfactory cure time. Despite that, those values will be considered to the characterization of the callus.

Lastly, the Gray sample presents a stiffness of 100 MPa, being the second most rigid material under test.

To conclude, in table 6 is presented the experimental Young's modulus obtained for every sample under test.

*Table 6. Calculated Young's modulus for the samples under test.*

<b>Material</b>	<b>Young Modulus (MPa)</b>
<b>Resin</b>	300
<b>Gray</b>	100
<b>Br 100:20</b>	8
<b>Br 100:23</b>	7
<b>Silicon</b>	2

Additionally, it was also characterized a sample of the tibia model [39]. The sample follows the guidelines dictated by the norm used, and it was characterized under the same test conditions as the previous samples.

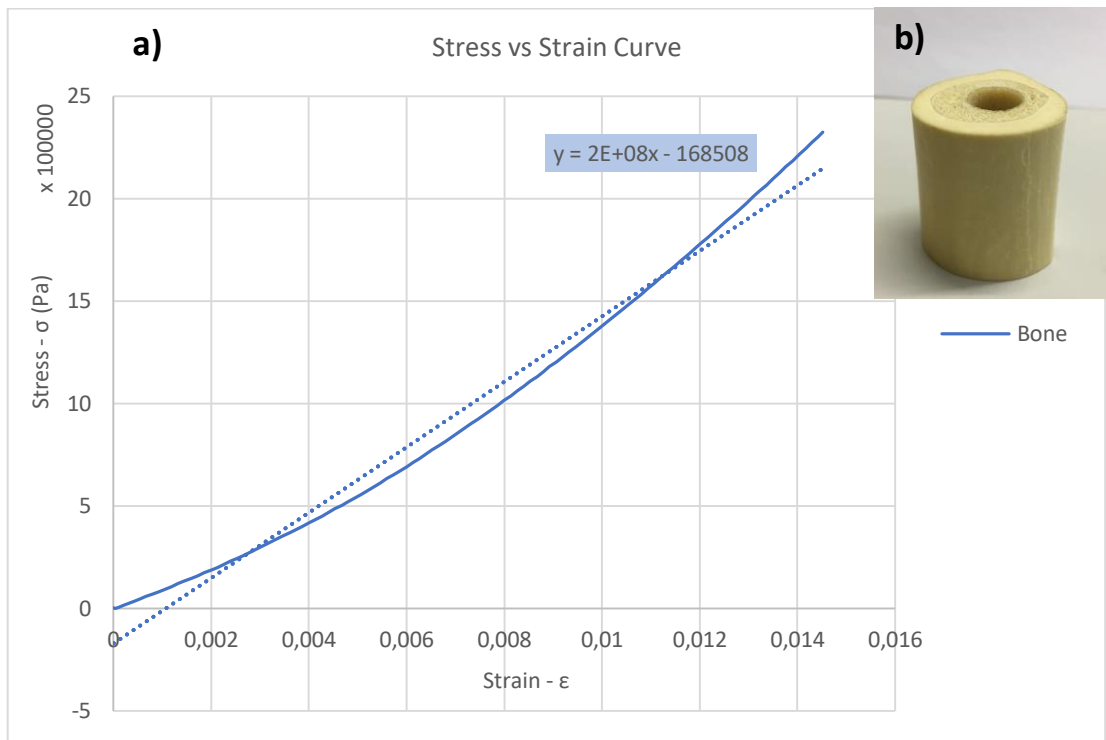


Figure 48. (a) Stress-strain curve for the bone sample (b) Bone sample.

The results showed a young's modulus to the synthetic bone of 200 MPa, value relatively low when compared to the one of the cortical bone reported in literature. This value can be explained by the characteristic rigidity of polyurethane foam, based material of the synthetic model; another explanation for the obtained value lasts with the low value of load reached, that was not enough to cause a significant strain in the sample.

#### 5.1.4. Callus' characterization

Despite the characterization of a hand-full of materials, only two phases can be identified when compared the several callus stages properties (Table 4, chapter 4.2.3.) to the mechanical properties of the materials under test (Table 6, chapter 5.1.3). Thereby, the selected samples were cutted into a 3 mm disc that can fill the gap created by the fracture.

*Table 7. Materials' assignment to their respective callus' phase.*

<b>Material</b>	<b>Assigned Callus' Phase</b>
<b>Br 100:23</b>	Fibrous Tissue Phase
<b>Gray</b>	Early Cartilage Phase
<b>Resin</b>	Cartilage Phase

## 5.2. Compression Test

The compression tests were performed into a synthetic bone coupled to an external fixator system. The fracture gap of 3 mm was considered; measure that was used in the numerical study and by the samples to simulate callus function in the previous subchapter.

An artificial model - Synbone tibia 1110 - was selected [39]. The model represents a right tibia with a cortical layer, a trabecular layer and a medullary canal present. In the ensuing Table 8, it is presented the dimensions of the model provided by the manufactures.

*Table 8. Synthetic bone measurements [39].*

<b>Synbone® Tibia 1110</b>	<b>Dimensions (mm)</b>
<b>Length</b>	387
<b>Tibia plateau width</b>	74
<b>Shaft diameter</b>	27
<b>Canal diameter</b>	8

Regarding to the external fixator, it is composed by a Hoffman 3 Modular External Fixator from Stryker® [41]. This system was used as a base for the FEM model fixator, and its dimensions were previously mention during the virtual model procedure explanation. The insertion of the pins in the synthetic bone and the assembly of the rest of the fixator was conducted by a specialized orthopaedist, what enables the montage as a realistic one.

The strain gauges were implemented in each rod of the fixator. The use of a strain gauge allows the analysis of the rod deformation while a load is applied. The selected strain gauges are a product by Micro-Measurements, a VPG Brand [56]. The final model can be seen in Figure 49.

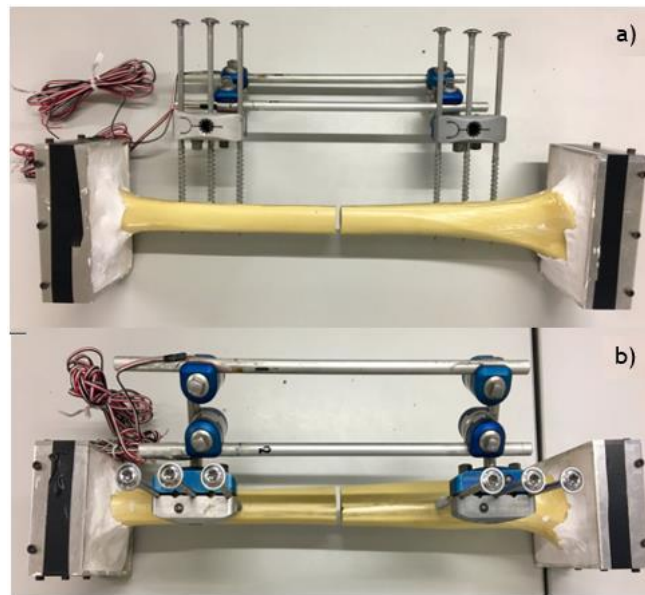


Figure 49. Bone and external fixator model, with strain gauges coupled.

The compression test was performed in the Instron EletroPuls E1000 [54], with a pre-load of 50 N until 1000 N at a crosshead speed of 5 N/s. The connection of the strain gauges to the *software* that collects and filters the data was made by a High-Speed USB portable Carrier, NI USB-9162, from National Instruments® [57]. The entire setup can be seen in Figure 50.

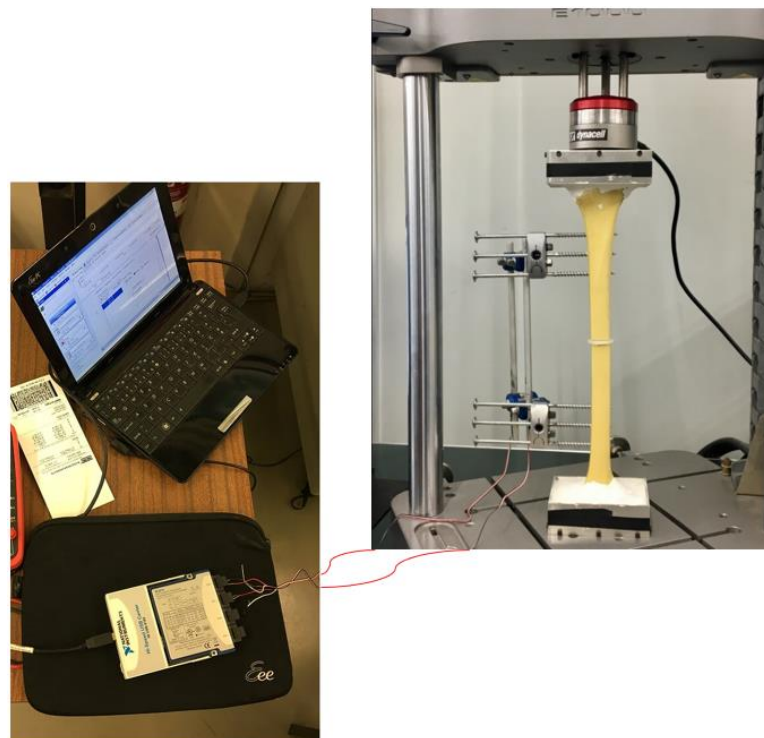


Figure 50. Test setup.





## Chapter 6. Results Presentation

In this chapter it will be presented the results obtained in the two phases of the project, discussing the limitations and difficulties experienced.

### 6.1. Results of the Finite Element Analysis

After simulating all the models created, with crescent properties of the fracture callus, there are several conclusions to argue. It is expected that, in an initial regeneration phase, the stress distribution in the rod will be higher than in the bone; as the callus regenerate, this stress is gradually decreased in the rod and increased in the bone. Regarding this statement, the main focus of the results was on the stress concentration at the callus, in the bone section surrounding the fracture and along the rod. The sections under analysis can be seen in Figure 51. Von Mises stress and displacement were chosen as parameters for the evaluation of the results obtained with FEA simulation. As mentioned before, the same attributes were held as the models were created; the only variable assumed was the callus properties, which was varied according to the regeneration phases' mechanical attributes.

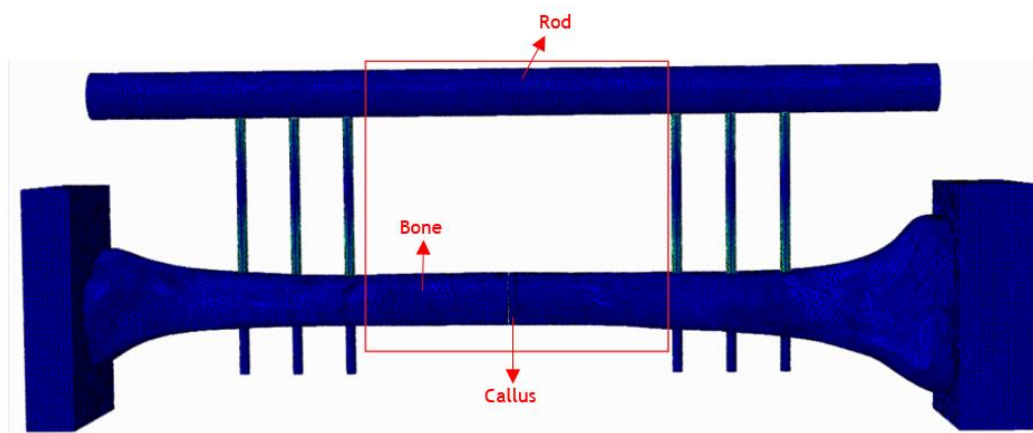


Figure 51. Sections under analysis: callus, bone section surrounding the fracture and callus.

The von Mises stress is a criterion that evaluates the maximum distortion energy of a material: a material starts to fail when the von Mises stress value approaches the material characteristic yield strength [58].

All the simulations, either for transversal and oblique fracture, global results can be seen in the images in Annex.

The graphic presented in Figure 52 represents the maximum values of the Von Mises stress in the regions of interest for the transversal fracture. To better preview the graphic behaviour, it was assumed a logarithmic scale in the callus' Young's modulus axis.

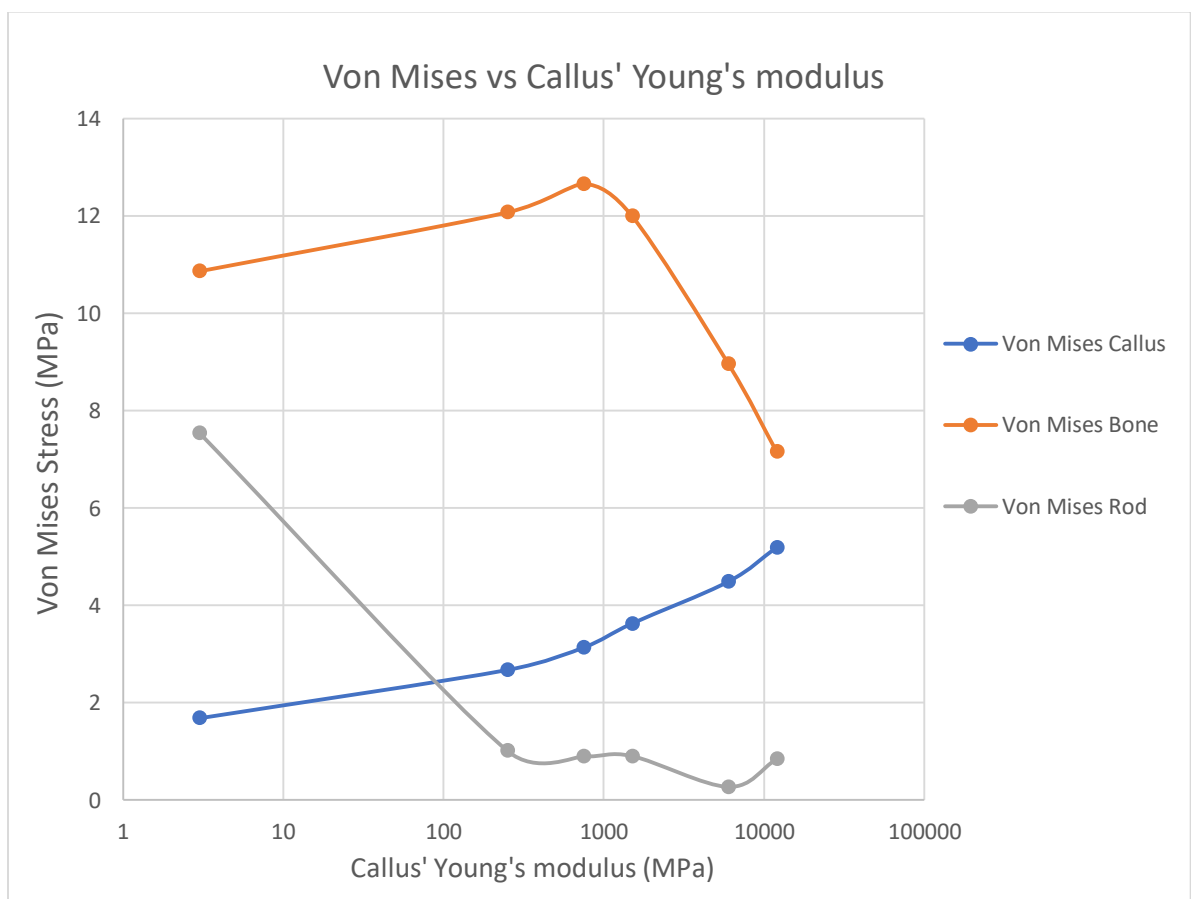


Figure 52. Representation of the Von Mises variation during transverse callus' regeneration.

As can be seen in Figure 52, all the main sections have different behaviours toward its maximum tensions distribution. The stress distribution at callus increased as its properties

become stiff; in other hand, the stresses in the rod decrease along the consolidation process; the stress distribution of the bone is variable, presenting an almost quadratic form, with an initial increase of stress, followed by an accentuated decrease after the 900 MPa mark of callus' Young's modulus.

Regarding to the callus, as previously mentioned, it presents a maximum Von Mises' rate almost proportional to its own Young's modulus value. The progression of the callus' stress distribution can be seen in Figure 53.

Concerning to the behaviour of the rod, the results show an expectable decreasing scheme: as the callus regenerates, the fixator starts to diminish its preponderance for the load accommodation, sharing gradually its efforts with the osseous structure. When the callus has 90 MPa of Young's modulus, the stress distribution becomes higher in the callus and it occur a stress reduction in the rod. That fact is graphically marked by the intersection of both the Von Mises' curves. The biomechanical meaning of that point of intersection is that the callus has now enough rigidity to support a primary state of union of the fractured bone. In Figure 54 can be figuratively seen the sudden decrease of the stress in the rod between the first and the second simulations, in an interval that includes the referred point. *Li et Al* [59] and Filardi [60] reported the transference of load between the fixator and the bone, when the callus begins to consolidate. It is mention the preponderant action of the external fixator in the load accommodation whilst the bone has no capacity to support the body weight, what corroborates the mentioned results.

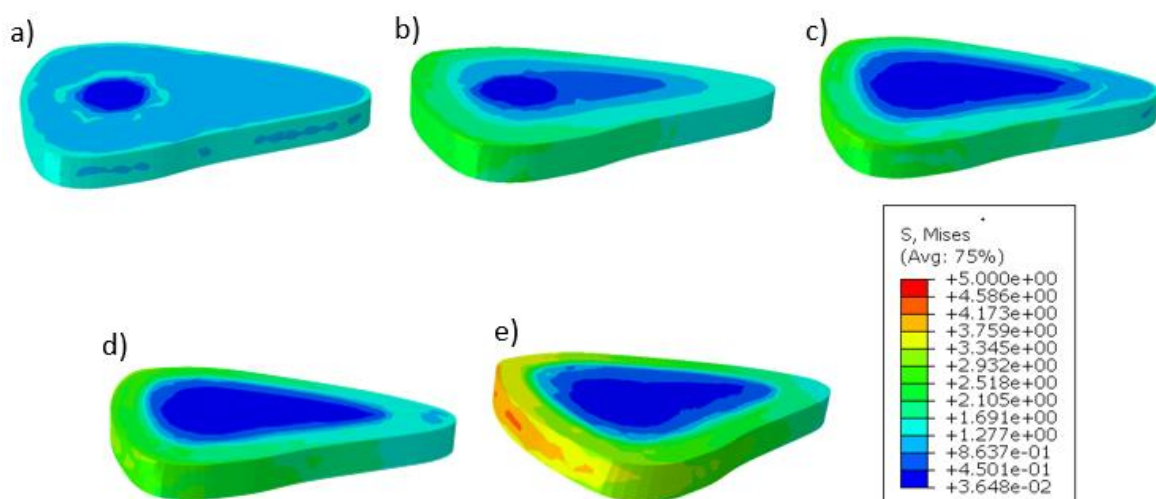


Figure 53. Von Mises stress distribution (MPa) when transverse callus has a Young's modulus of (a)3MPa, (b)250MPa, (c)750MPa, (d)1500MPa and (e)6000MPa.

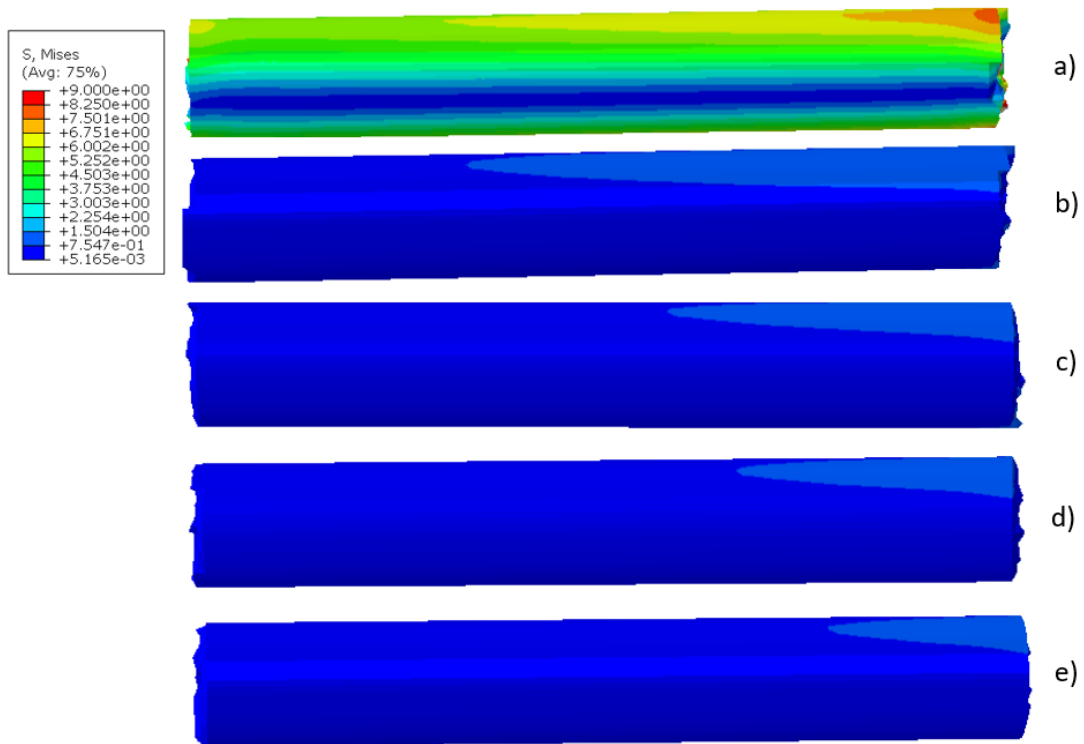


Figure 54. Von Mises stress distribution (MPa) at Rod when transverse callus' has a Young's modulus of (a) 3MPa, (b) 250MPa, (c) 750MPa, (d) 1500MPa and (e) 6000MPa.

Concerning to the stress distribution of the bone, the results show that its behaviour is not as regular as the remaining. There about 900 MPa, it has a crescent linear performance: as the callus' properties are recovered, the bone starts to regain its ability of support, induced a higher stress concentration in that stage [59].

After the 900 MPa callus' Young's modulus the Von Mises stresses progressively decrease. The point where the bone reaches the highest stress distribution is, coincidentally, the moment where the callus properties match the trabecular bone properties. This can indicate that the callus accommodates and supports a higher stress concentration as it recovers its mechanical properties. At this phase, the bone union is considered consolidated. The results also show that, in that point, the stress at the rod tends to stabilize, what proves the advance state of union of the bone structure. There are several studies reported with intramedullary nails or other fixation devices, but no projects were found with similar conditions as the assumed in this project, so the results cannot be compared because of the lack of precedents.

The results show that the values of the stress at the bone were higher than the stresses at the rod, in all phases of healing. The fact was not the expectable, because the intention of insert an external fixator is to reduce the bone's mechanical solicitation, conferring more stability along the osseous structure, fomenting an effective consolidation. With that said, the fixator in an early callus' phase should accommodate more stresses than the bone. That occurrence may happen due to the broad rigidity difference between both the materials: as the aluminium has a Young's modulus far superior to the bone one, the tensions present in the osseous structure can be wrongly amplified when compared to the stress distribution in the rod.

The stress distribution for the bone surface connected with the callus can be seen in Figure 55.

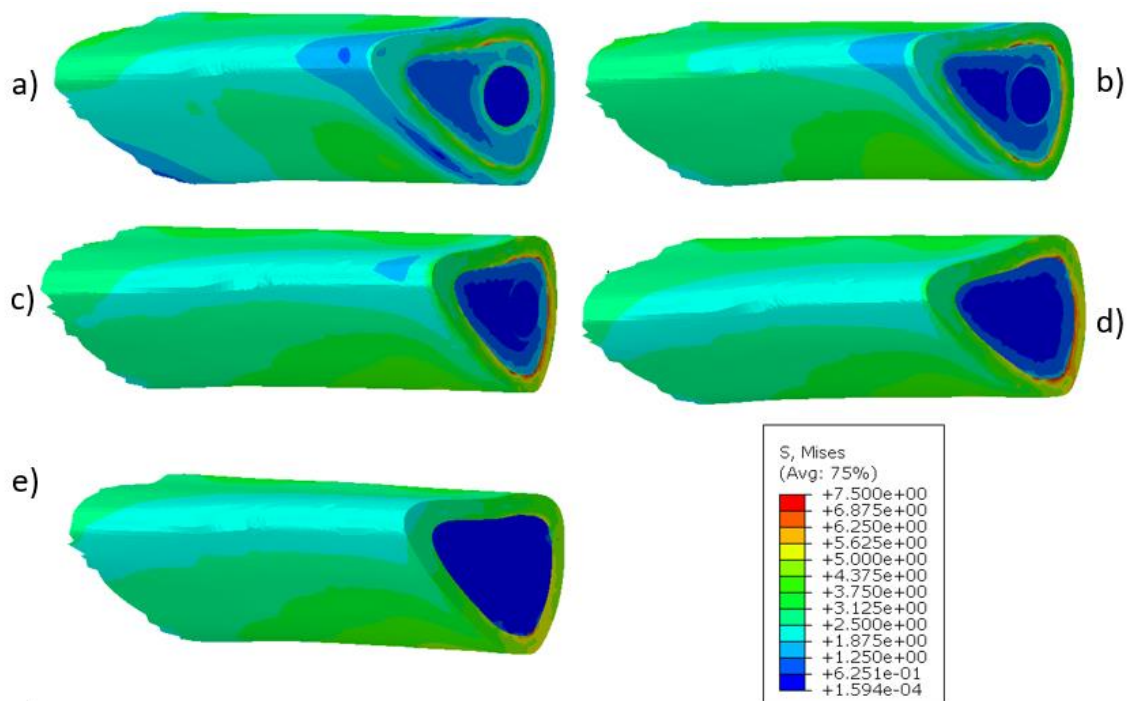


Figure 55. Bone's upper interface with callus stress distribution when transverse callus' has a Young's modulus of (a)3MPa, (b)250MPa, (c)750MPa, (d)1500MPa and (e)6000MPa.

In the most advance callus' Young's modulus value, it is possible to predict that the stress of the bone is converging with the same parameter in the callus. It was made a simulation using a Callus' Young's modulus of 12000 MPa to better describe the behaviour of the callus and bone, and thus predict at which point those curves intersect. It was assumed a linear regression of both graphs, that could be seen in Figure 56.

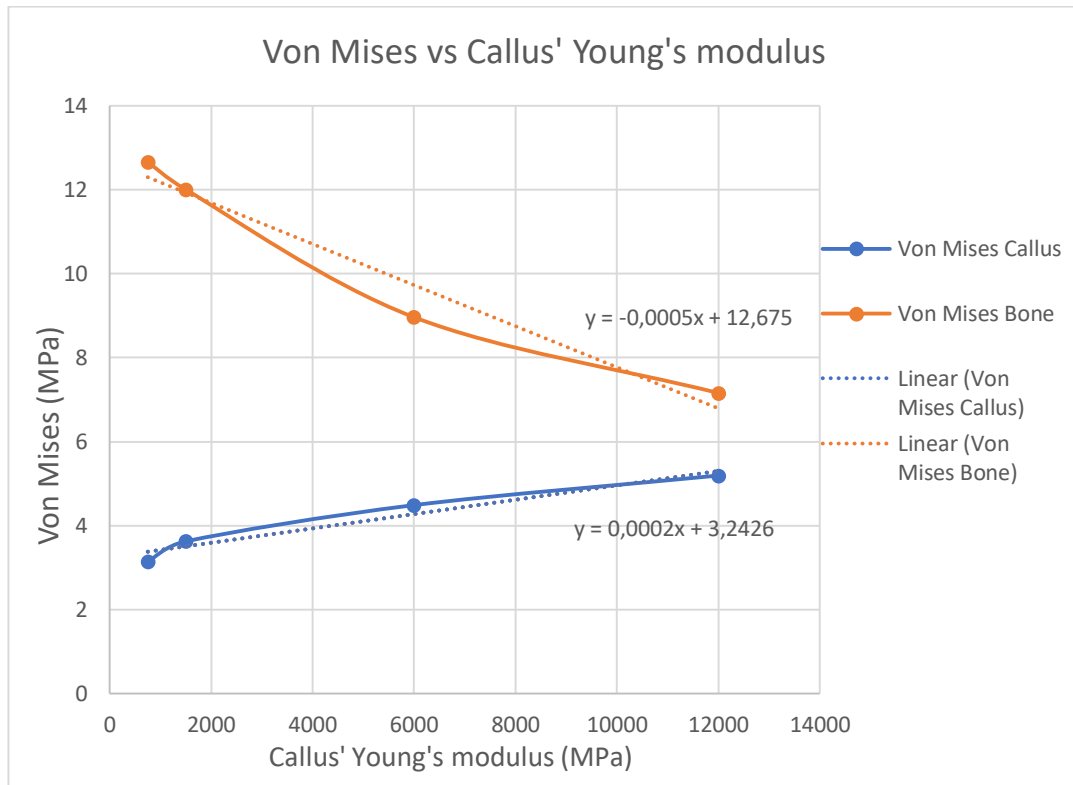


Figure 56. Transverse callus' and Bone's Von Mises graph final phase behaviour.

By equation of both linear functions, it has been calculated that they cross nearly the 13500 MPa. With a minor error, that value can be approximated to the cortical bone Young's modulus. The biomechanical meaning of this assumed intersection is that the callus fully restores its osseous properties and no longer exists.

Additionally, it was traced the curves for the displacement variations (Figure 57) in the sites previously mentioned and highlighted. It is easily noticed that all the structures have similar displacement behaviour, but the rod has a lower maximum value. That fact is attributed due to the high rigidity properties that the constitutive aluminium presents.

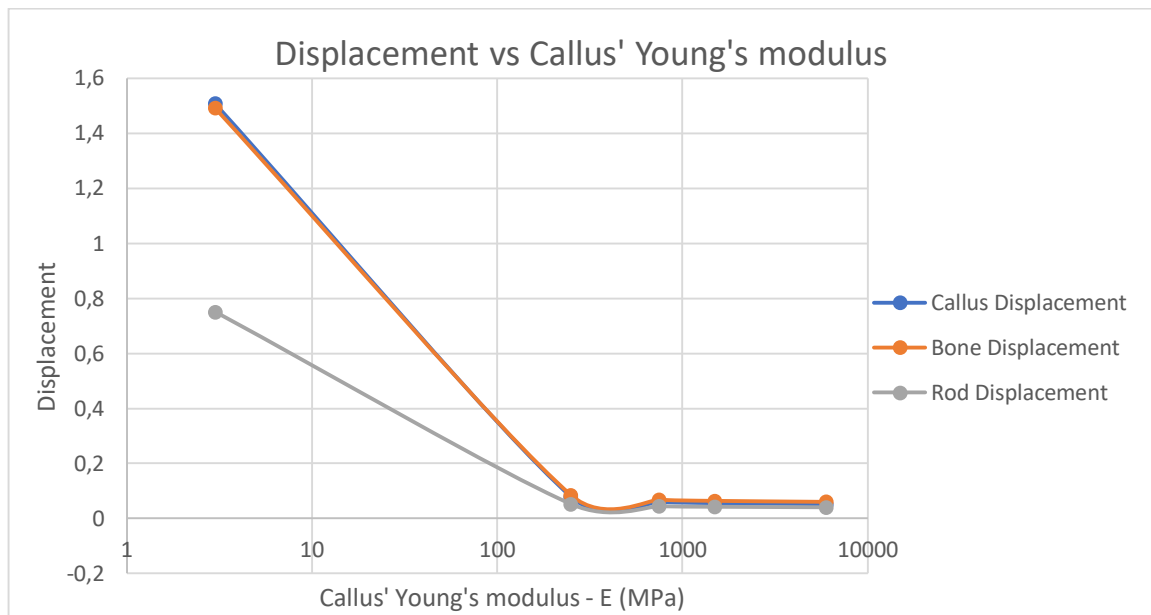


Figure 57. Displacement variation during transverse callus' regeneration.

Regarding to the oblique fracture, the maximum Von Mises stress values in the regions of interest can be seen in Figure 58.

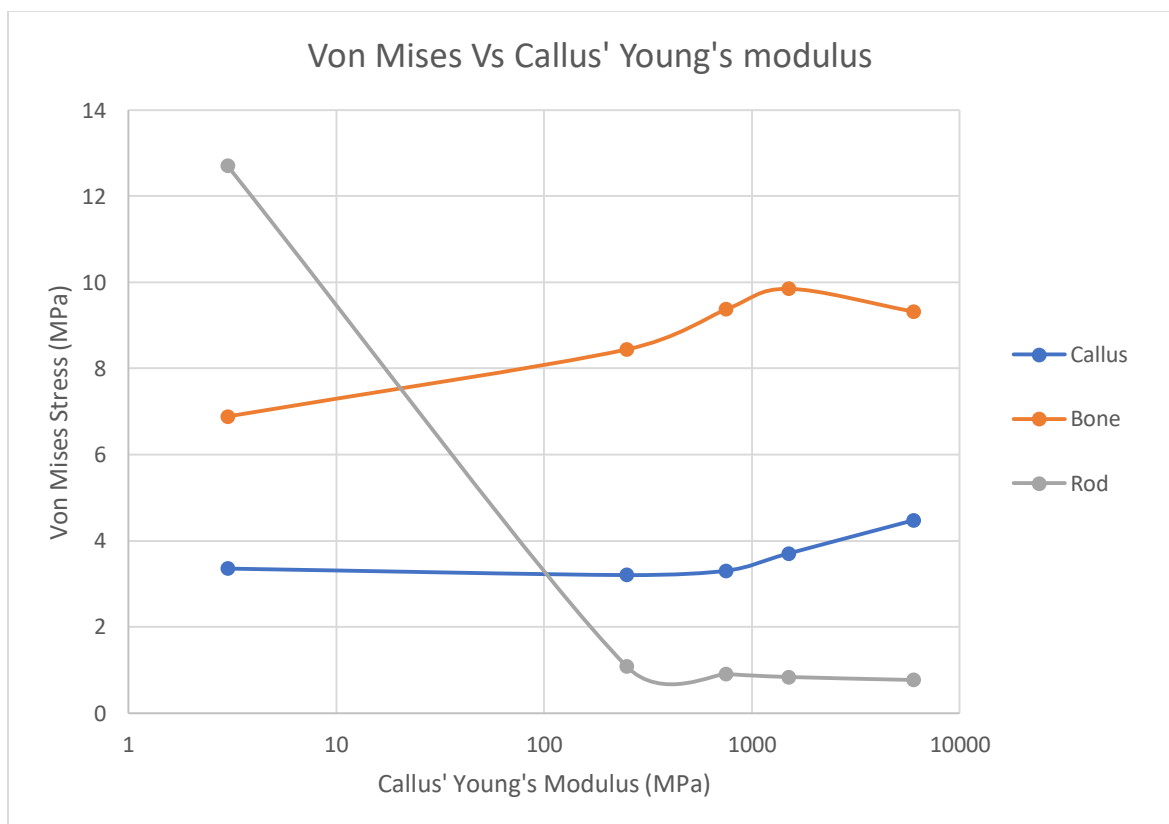


Figure 58. Representation of the Von Mises variation during oblique callus' regeneration.

The behaviour of the three regions is very similar to its correspondent for the transverse fracture: the callus' region presents an increasing stress behaviour; the rod's stress decreases along the callus regeneration; and the bone's curve as a similar form as the one in the transverse fracture analysis, presenting a change of direction in the same phase. The cross between the rod and callus curves occurs around the 100 MPa of callus' Young's modulus, assuming the callus a higher preponderance in the load accommodation than the rod from this phase on.

Comparing both fractures Von Mises' stress graphics, it can be noticed a difference in the relative position, in an early callus' phase, between the maximum Von Mises stress in the rod and in the bone. In the oblique fracture case, the model with an initial callus induced a high stress concentration in the rod; on the other hand, this stress has a lower value at the bone. Owe the fixator the purpose of sustain the bone's mechanical solicitation in a premature callus phase, the higher initial stress value in the rod is acceptable and expectable. Around 80 MPa of callus' Young's modulus, the rod loses stiffness and the fracture recovers rigidity, hence the ability to transmit load.

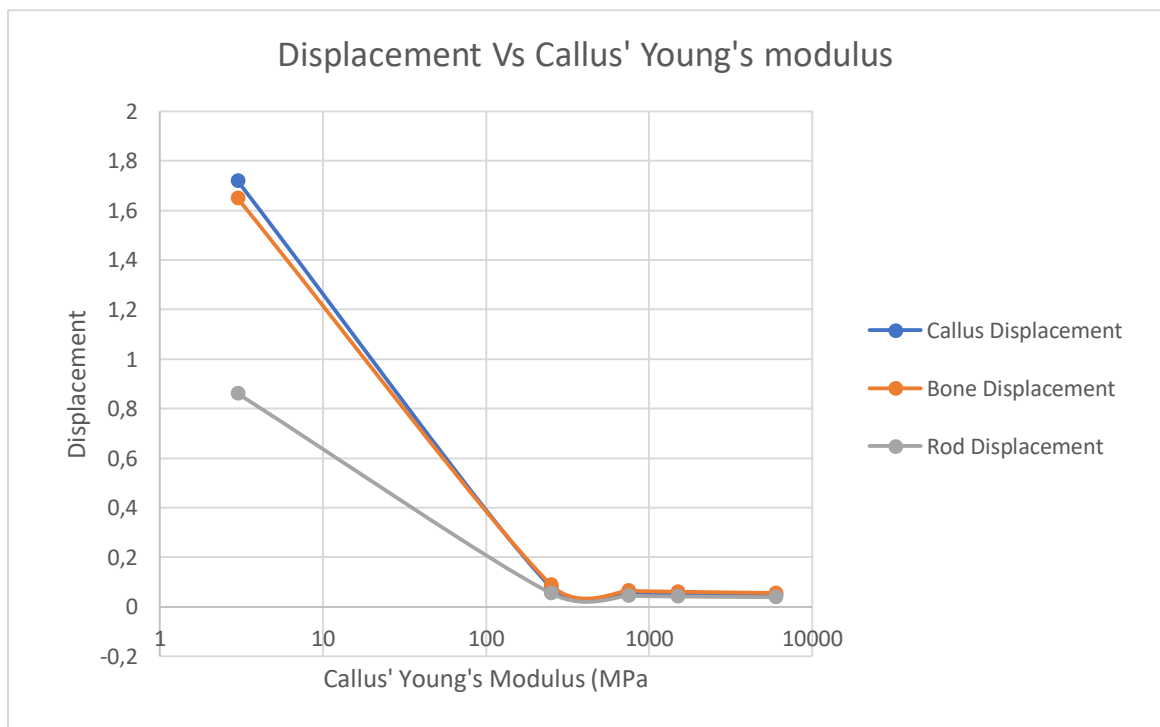


Figure 59. Displacement variation during oblique callus' regeneration.



As can be seen in Figure 59, the displacement in all the interest regions tend to zero as the callus consolidate. The displacement variable is a manner to understand that along the callus properties arises and the bone consolidates, there are a synergy between all the components to attenuate the load, due to its higher rigidity.

## 6.2. Results of the Compression tests

For the compression tests, it was given different names to distinguish the two strain gauges' results. Thereby, they were names according to the rod that they were attach to, as can be seen in Figure 58.

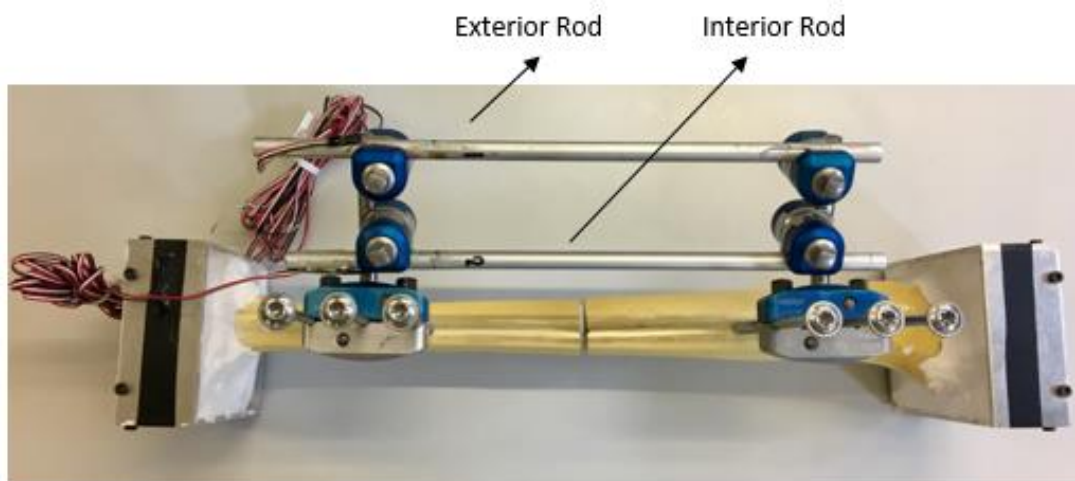


*Figure 60. Denomination of the Strain Gauges.*

After the execution of the tests under the guidelines previously mentioned, all the measurements were aggregate in Figure 59. The mentioned graphic shows the Deformation values for three types of callus, representative of different regenerative callus' phases. As mentioned before, the Br10023 material represents a primary fibrous tissue phase; the "Gray sample" represent an early secondary cartilage phase; and the epoxy resin mimics an intermediate stage of the cartilage phase.

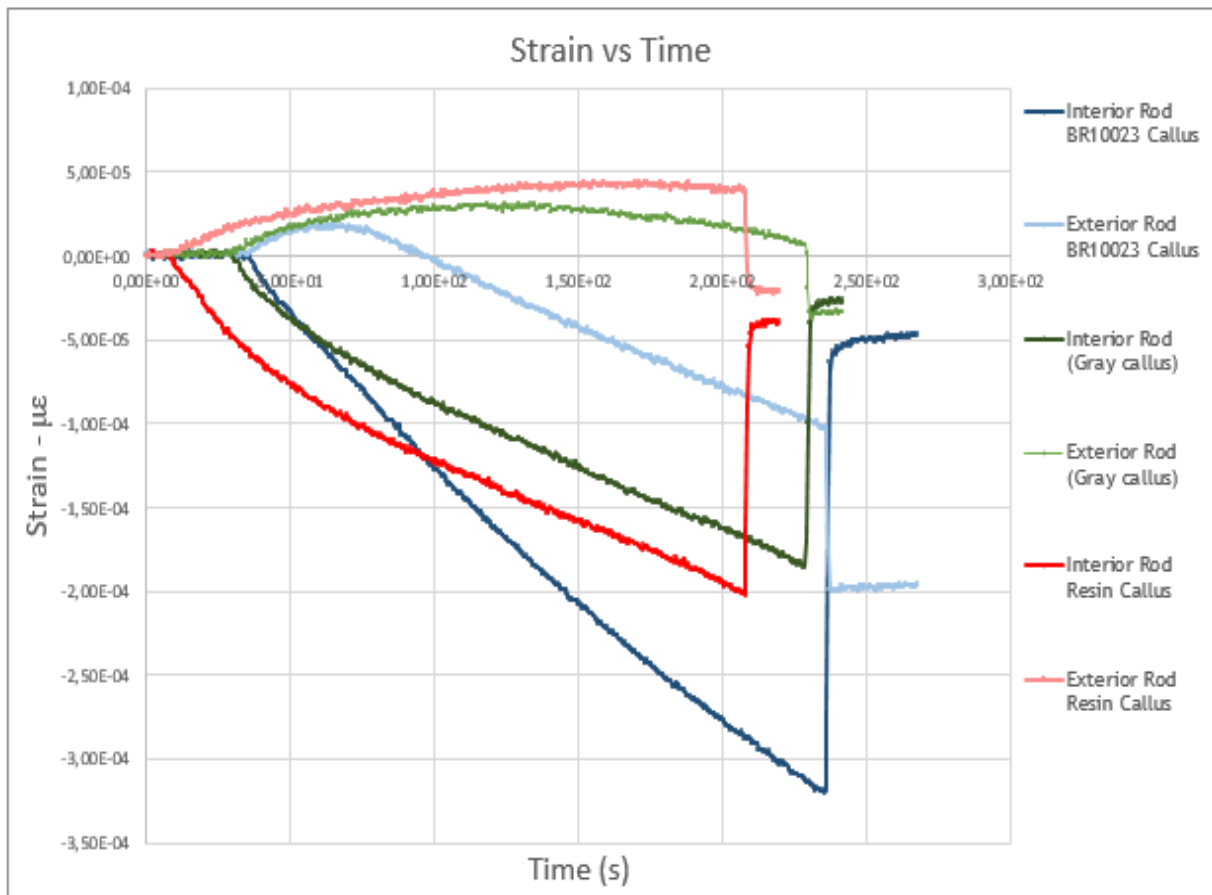


Figure 61. Strain Gauges' measurements in the compression test of the Tibia model.

Concerning to the callus formed by the Br10023, and represented by the blue set of curves: being a primary callus' phase, it is expectable that this will be the simulation where the Rods deform more. The dark blue line, representing the fixator's interior rod, asserts that statement by lodging the higher value, in modulus, between all the measurements done. That means that, when applied a defined force to a fractured bone, the external fixator will suffer a biggest amount of deformation the more premature is the callus.

The great advantage of having a bicomponent rod is the sharing of deformation between its components: as can be seen too, between all the exterior rod's measure, the light blue line is the one that presents the biggest amount of deformation. That fact lasts with the higher amount of load that a fixator needs to accommodate in an early regeneration phase, while the osseous support is clearly insufficient. It is also noticed that the Br10023 exterior Rod presents a final negative value, when the load is maximum; the interpretation of the curve's behaviour

may denote a bending suffered at certain point. *Torcasio et Al.* [61] and *Funk et Al.* [62] reported the possible production of deformation and bending while an axial compressive load is applied in the bone.

After the cessation of the load, both the interior and exterior rods have their deformation curve converging. The converge point implies the overall deformation of the structure.

Regarding to the “Gray sample” and the Resin callus’ like, their divergences are minimum, what denotes that both materials represent the same regeneration phase. Nevertheless, and because the Resin represents a more advance stage, some commentaries need to be done.

In both cases, it is visible that their exterior rods remain in the positive zone of the graphic: the physical meaning of that occurrence is that the applied load is not enough to cause a bending in the auxiliary frame. It is important to denote that the light green curve presents a switch of direction, what proves that, despite a bending not occur, it would not be far from happening.

Relatively to the interior Rods, both present a deformation value lower than the one measured in the Br10023 callus. The more rigid the material constituent of the callus, a less amount of deformation is caused in the fixator, due to the progressive recovery of the mechanical properties by the bone [59][60]. The doubtful measurement is brought by the comparison of the Resin and “Gray” calluses’ interior rod, where the minimum value is higher for the dark green line. Well, if the resin mimics a more advance consolidation phase, its deformation should be lower in modulus, and that does not occur.



# Chapter 7. Conclusion and future work

## 7.1. Conclusion

The main intention of this project lasts with the comprehension of the bone consolidation process when subjected to a fracture, allied to a monitoring that could evaluate each patient's progression singly, due to the high variability of consolidation in each case. Being the tibia the second largest and strongest bone in the human body, therefore broadly susceptible to a hard strike, it was the long bone chosen to be tested. The knowledge of the tibia's anatomy was fundamental to its construction, allowing its division into three layers with distinctive mechanical properties. The symbiosis between an experimental component and a 3D finite element analysis allows the characterization of the overall system behaviour when subjected to a specific load.

Several materials were subjected to compression tests to obtain the characteristic mechanical properties. The choice of the tested materials was made taken into account the flexibility of its mechanical properties values only diversifying the substances' ratios. Unfortunately, the range of elasticity was not as vast as predictable, what just allow the characterization of two callus' regeneration phases. The assay protocols and guidelines were accomplished and used for all the compression tests, including the ones executed on the tibia with fixator model. Resorting to the obtained results, it was considered that the objective was achieved: the rod's strain gauges' results materialize the expected behaviour of the fixator. Along the callus' consolidation, the preponderance and tensions present on the rods decrease, conferring some autonomy along time to the osseous system.

Concerning to the FEA, the model was constructed taken into account the exact topology of the tibia bone, and an approximation of the inside structure of it. The simplified design of the external fixator was based in a real fixator, with accurate dimensions attached. The numerical simulation by the finite element method turned out an essential tool to better describe the behaviour of the various model regions along the consolidation. The stress response to the several test conditions allow the tracing of the characteristic behaviour

associated to the callus' regeneration process. The concordance between the overall results' interpretation between the numerical simulation and the compression tests allows the validation of the model, what enable the properties' variation of the materials in order to simulate different conditions. The obtained results show the divergence of behaviours of the several interest areas: the callus presents an almost linearly crescent distribution of tensions as its Young's modulus increase; in opposite way, the fixator's rod decrease its overall tensions as the callus' properties are recovered; the behaviour of the bone is more complex than the other, presenting a variation of behaviour along the callus Young's modulus. The bone as an initial increase of tensions, following the behaviour adopted by the callus, followed by a sudden decrease nearly by the moment the callus' properties match the trabecular bone's Young's modulus ( $E=900$  MPa). It is concluded that the fixator accomplished its function of support, reducing the tensions that the osseous system had to maintain.

## 7.2. Future work

Despite the satisfactory results obtained along the dissertation, several aspects can be improved:

- The 3D model geometry could be improved to represent a more faithful interaction between the layers inherent to the bone;
- Cortical bone was assigned using linear isotropic material properties, what consents with the model simplification, but not with the real material behaviour. Thereby, an orthotropic behaviour should be adopted;
- The force applied in the tibial plateau was kept uniform along its area. Changing the load distribution to a more reliable one could exhibit better performance results and approximate the simulation to the real human performance;
- A set of materials with different rigidity could be considered, in the future, to allow the characterization of all the callus' regeneration phases;
- A dynamic analysis could be implemented for both compression and finite element analysis;
- The fixator geometry used in the FEA was a simplified version of a real fixation system. Thereby, by future prospects, a fixator more similar to the Hoffman one should be used.
- A better treatment of the results should be considered: per example, an analysis of the variance of the Von Mises stress along the bone may produce different conclusions.

## References

- [1] C. Starr and B. McMillan, *Human biology*. Brooks/Cole Cengage Learning, 2014.
- [2] J. G. Betts, P. Desaix, E. Johnson, J. Johnson, O. Korol, and D. Kruse, *Anatomy & Physiology Vol. 1*. OpenStax College, 2013.
- [3] BioDigital Human Platform, “Human Anatomy and Disease in Interactive 3D.” [Online]. Available: <https://human.biodigital.com/index.html>. [Accessed: 07-Feb-2019].
- [4] G. Bourne, *The biochemistry and physiology of bone*. Elsevier, 1976.
- [5] C. Crowder and S. D. Stout, *Bone histology: an anthropological perspective*. CRC Press, 2011.
- [6] L. Aiello and C. Dean, *An introduction to human evolutionary anatomy*. Elsevier, 2002.
- [7] K. T. Patton, *Anatomy and Physiology*. Elsevier Health Sciences, 2015.
- [8] D. V. Knudson, *Fundamentals of biomechanics*. Kluwer Academic, 2003.
- [9] A. Codea and C. Vicentini, *Anatomia Humana*. Clube de Autores, 2009.
- [10] S. Standring and N. R. Borley, *Gray’s Anatomia: a Base Anatômica da Prática Clínica*. Elsevier, 2010.
- [11] R. Oftadeh, M. Perez-Viloria, J. C. Villa-Camacho, A. Vaziri, and A. Nazarian, “Biomechanics and Mechanobiology of Trabecular Bone: A Review,” *J. Biomech. Eng.*, vol. 137, no. 1, p. 010802, Jan. 2015.
- [12] R. C. Henrikson, G. I. Kaye, and J. E. Mazurkiewicz, *Histology*. Williams & Wilkins, 1997.
- [13] R. Setiawati and P. Rahardjo, “Bone Development and Growth,” in *Osteogenesis and bone regeneration*, IntechOpen, 2018.
- [14] C. Molnar and J. Gair, *Concepts of Biology-1st Canadian Edition Molnar Class*. 2012.
- [15] A. F. Tencer and K. Johnson, *Biomechanics in orthopedic trauma : bone fracture and fixation*. M. Dunitz, 1994.
- [16] W. Riser, *History of small animal orthopaedics*. 1985.

- [17] B. D. Browner and P. G. Trafton, *Skeletal trauma*. Saunders, 2009.
- [18] B. D. Browner, J. B. Jupiter, C. Krettek, P. Anderson, and ClinicalKey., *Skeletal trauma : basic science, management, and reconstruction*. Elsevier, 2009.
- [19] G. E. Wnek and G. L. Bowlin, *Encyclopedia of biomaterials and biomedical engineering*. Informa Healthcare, 2008.
- [20] K. Khatri, D. Lakhota, V. Sharma, G. N. Kiran Kumar, G. Sharma, and K. Farooque, "Functional Evaluation in High Energy (Schatzker Type V and Type VI) Tibial Plateau Fractures Treated by Open Reduction and Internal Fixation," 2014.
- [21] F. Magerl, "Current Concepts of External Fixation of Fractures," in *Current Concepts of External Fixation of Fractures*, Springer Berlin Heidelberg, 1982, pp. 353-366.
- [22] L. N. Solomin, *The basic principles of external fixation using Ilizarov device*. Springer, 2008.
- [23] L. N. Solomin, *The basic principles of external skeletal fixation using Ilizarov and other devices*. Springer, 2012.
- [24] PCB Load & Torque: a PCB Group Company, *Load Cell Handbook. A Technical Overview and Selection Guide*. PCB Load & Torque: a PCB Group Company, 2014.
- [25] J. L. Cunningham, J. Kenwright, and C. J. Kershaw, "Biomechanical measurement of fracture healing," *J. Med. Eng. Technol.*, vol. 14, no. 3, pp. 92-101, Jan. 1990.
- [26] R. Hente, J. Cordey, and S. M. Perren, "In vivo measurement of bending stiffness in fracture healing," *Biomed. Eng. Online*, vol. 2, no. 1, p. 8, Mar. 2003.
- [27] D. A. Baga, V. Protopappas, D. I. Fotiadis, and A. Likas, "A Wearable Ultrasound Device for the Monitoring and Acceleration of Bone Fracture Healing."
- [28] W. H. Ong, L. Salvino, M. Russ, W. K. Chiu, and Z. Chiu, "Human SHM-healing assessment of an externally fixated fractured femur." NDT Internet Publishing, pp. 2718-2726, 2016.
- [29] J. D. Currey, *Bones : structure and mechanics*. Princeton University Press, 2002.
- [30] W. Jee, *Integrated Bone Tissue Physiology: Anatomy and Physiology*, vol. 45. Phys Ther, 1965.
- [31] A. D. Pria Bankoff, "Biomechanical Characteristics of the Bone," *Hum. Musculoskelet. Biomech.*, 2012.
- [32] A. Sharir, M. M. Barak, and R. Shahar, "Whole bone mechanics and mechanical testing," *Vet. J.*, vol. 177, no. 1, pp. 8-17, Jul. 2008.
- [33] R. Arshad, "Master Thesis Modelling Inhomogeneities within the Human," University of Stuttgart, 2004.
- [34] R. Huiskes and E. Y. Chao, "A survey of finite element analysis in orthopedic biomechanics: the first decade.," *J. Biomech.*, vol. 16, no. 6, pp. 385-409, 1983.



- [35] J. Fish and T. Belytschko, *A first course in finite elements*. John Wiley and Sons LTD, 2007.
- [36] K.-J. Bathe and E. L. Wilson, *Numerical methods in finite element analysis*. Prentice-Hall, 1976.
- [37] S. and T. I. B. National Aeronautics and Space Administration (NASA), *Tenth NASTRAN Users' Colloquium: proceedings of a colloquium held at New Orleans, Louisiana - United States. National Aeronautics and Space Administration. Scientific and Technical Information Branch*. NASA, 1982.
- [38] H. Arjmand *et al.*, "Mechanical Metrics of the Proximal Tibia are Precise and Differentiate Osteoarthritic and Normal Knees: A Finite Element Study," *Sci. Rep.*, vol. 8, no. 1, p. 11478, Dec. 2018.
- [39] "1110 Archives - SYNBONE." [Online]. Available: <https://www.synbone.com/product-tag/1110/>. [Accessed: 07-Feb-2019].
- [40] S. J. Song and B. O. Jeong, "Three-dimensional analysis of the intramedullary canal axis of tibia: clinical relevance to tibia intramedullary nailing," *Arch. Orthop. Trauma Surg.*, vol. 130, no. 7, pp. 903-907, Jul. 2010.
- [41] Stryker®, "Hoffmann 3 - Modular External Fixation. Operative Technique," pp. 0-11.
- [42] H. Deng, Y. Liu, C. Guo, and Di Chen, *Current Topics in Bone Biology*. World Scientific, 2005.
- [43] H. Bougherara *et al.*, "Biomechanical properties of an intact, injured, repaired, and healed femur: An experimental and computational study," *J. Mech. Behav. Biomed. Mater.*, vol. 16, pp. 121-135, Dec. 2012.
- [44] G. Lowet, X. Dayuan, and G. Van Der Perre, "Study of the vibrational behaviour of a healing tibia using finite element modelling," *J. Biomech.*, vol. 29, no. 8, pp. 1003-1010, 1996.
- [45] A. Mehboob, H. Mehboob, J. Kim, S. H. Chang, and F. Tarlochan, "Influence of initial biomechanical environment provided by fibrous composite intramedullary nails on bone fracture healing," *Compos. Struct.*, vol. 175, pp. 123-134, Sep. 2017.
- [46] C. Comte and J. von Stebut, "Microprobe-type measurement of Young's modulus and Poisson coefficient by means of depth sensing indentation and acoustic microscopy," *Surf. Coatings Technol.*, vol. 154, no. 1, pp. 42-48, May 2002.
- [47] J. Davis, *Tensile testing*. ASM International, 2004.
- [48] N. Phate, R. Nareliya, V. Kumar, and A. Francis, "Three-Dimensional Finite Element Analysis of Human Tibia Bone," *Int. J. Sci. Res. Eng. Technol.*, vol. 3, no. 1, pp. 2278-882, 2014.
- [49] "Altropol Kunststoff GmbH > ProtoFlex." [Online]. Available: <http://www.altropol.de/en/produkte/neukadur-polyurethansysteme/protolflex/>. [Accessed: 06-Mar-2019].

- [50] Sicomin, "SR 1500 Epoxy laminating system," 2014.
- [51] Z. S. P. A. H. Division, "HT 33 TRANSPARENT: Technical Data Sheet 1. Description and Main Features."
- [52] DuPont, "Teflon S Coatings."
- [53] ASTM standard D1621, "Standard Test Method for Compressive Properties Of Rigid Cellular Plastics," *ASTM Int.*, pp. 5-8, 2004.
- [54] Instron, "ElectroPuls™ | E1000 All-Electric Dynamic Test Instrument," 2014.
- [55] R. Zdero, *Experimental methods in orthopaedic biomechanics*. Academic Press, 2017.
- [56] Micro-Measurements, "General Purpose Strain Gages- Linear Pattern," 2017.
- [57] N. Instruments, "NI USB-9162 Portable Bus-Powered USB Carrier for NI C Series I/O Modules,". National Instruments, 2013.
- [58] M. B. Sternick, D. Dallacosta, D. Á. Bento, and M. L. do Reis, "Relação entre rigidez de fixador externo e quantidade de pinos: análise computacional por elementos finitos," *Rev. Bras. Ortop.*, vol. 47, no. 5, pp. 646-650, Oct. 2012.
- [59] J. Li, X. Zhao, X. Hu, C. Tao, and R. Ji, "A finite element analysis for monitoring the healing progression of fixator-bone system under three loading conditions," *Biomed. Mater. Eng.*, vol. 29, no. 4, pp. 473-483, 2018.
- [60] V. Filardi, "The healing stages of an intramedullary implanted tibia: A stress strain comparative analysis of the calcification process," *J. Orthop.*, vol. 12, pp. S51-S61, Oct. 2015.
- [61] A. Torcasio *et al.*, "3D characterization of bone strains in the rat tibia loading model," *Biomech Model Mechanobiol*, vol. 11, pp. 403-410, 2012.
- [62] J. R. Funk and J. R. Crandall, "Calculation of Long Bone Loading Using Strain Gauges."

## Annex

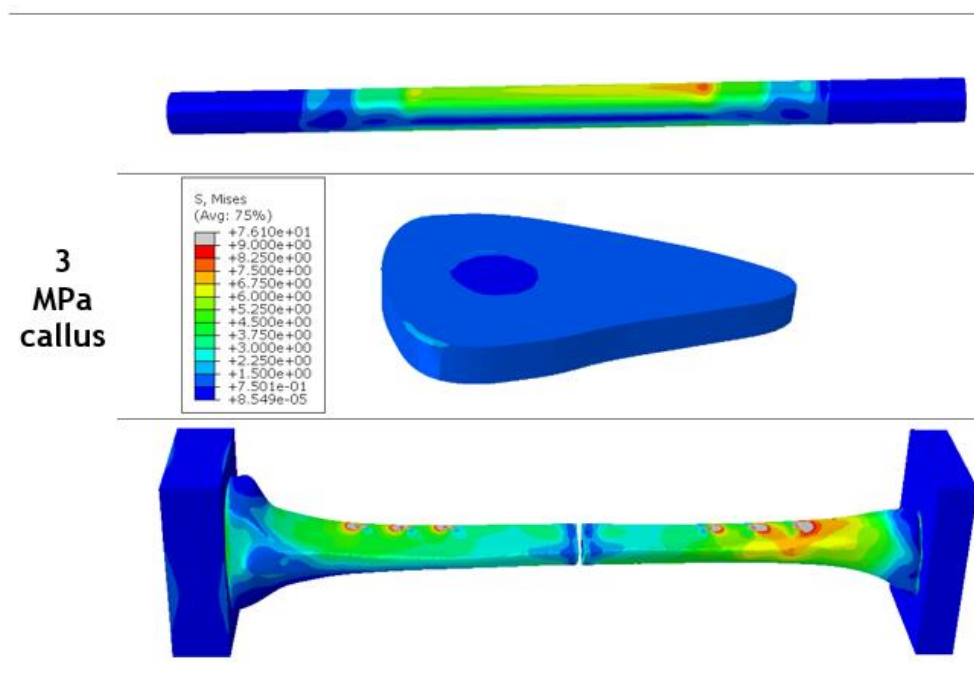


Figure 62. Von Mises' distribution for a transversal fracture with a Young's modulus of 3 MPa. Fixator's rod at the top; callus in the middle; bone structure down.

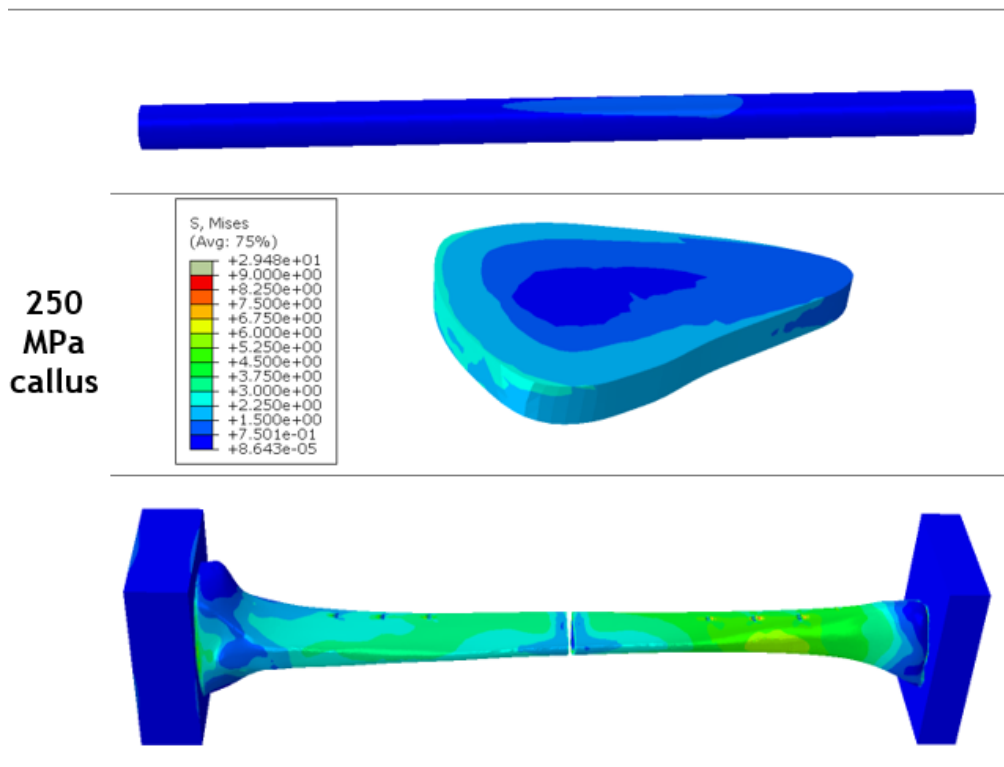


Figure 63. Von Mises' distribution for a transversal fracture with a Young's modulus of 250 MPa. Fixator's rod at the top; callus in the middle; bone structure down.

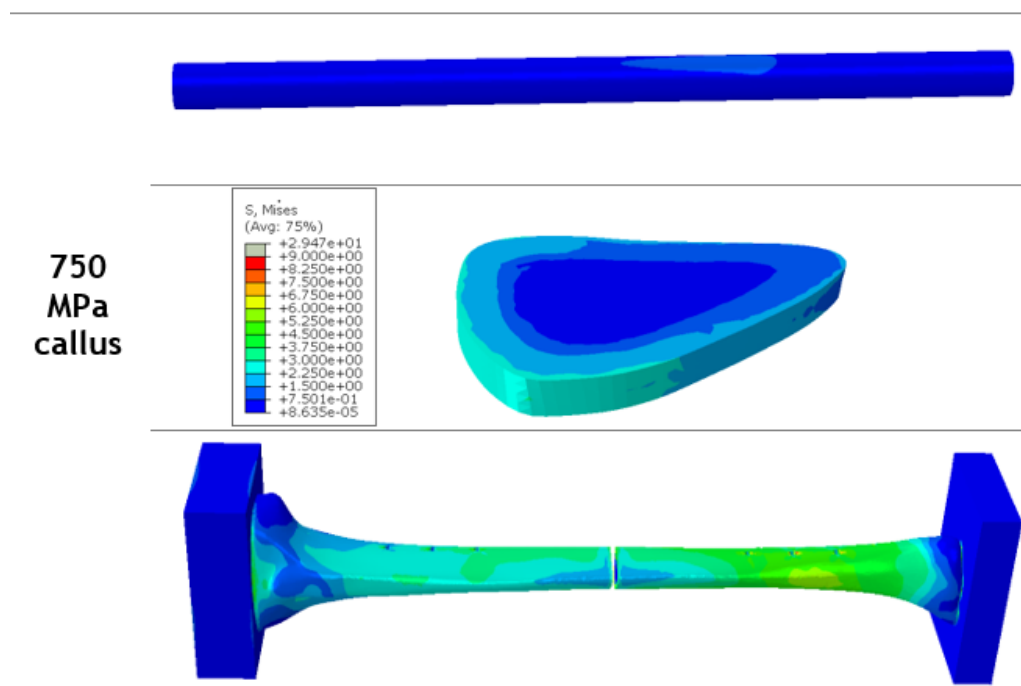


Figure 64. Von Mises' distribution for a transversal fracture with a Young's modulus of 750 MPa. Fixator's rod at the top; callus in the middle; bone structure down.

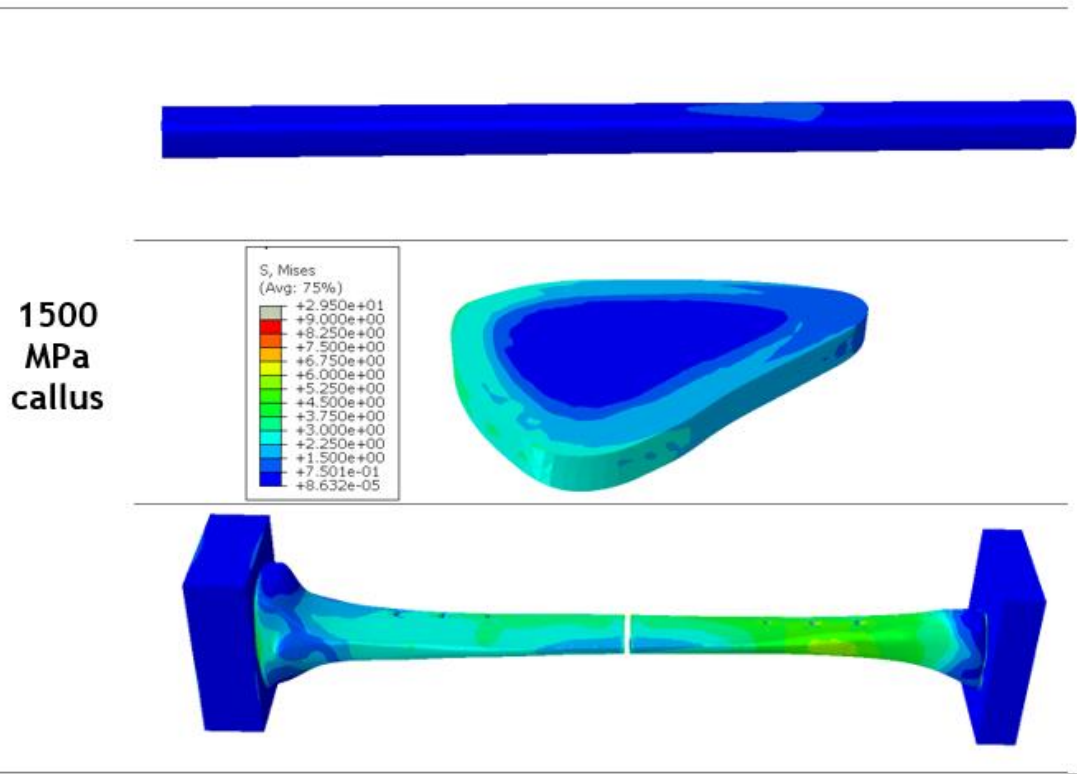


Figure 65. Von Mises' distribution for a transversal fracture with a Young's modulus of 1500 MPa. Fixator's rod at the top; callus in the middle; bone structure down.

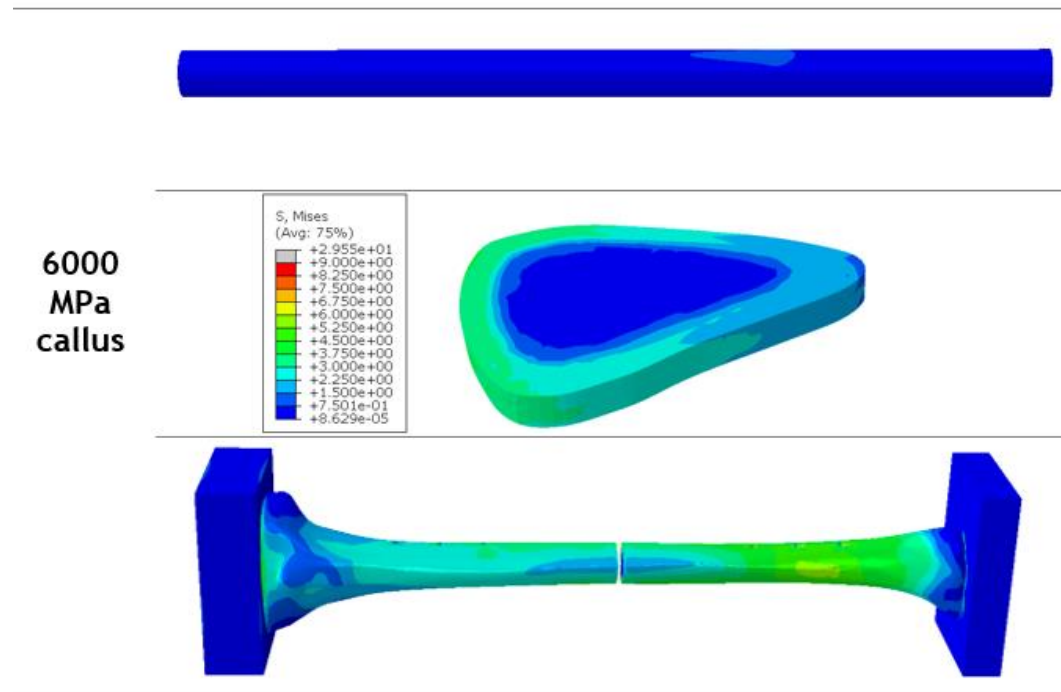


Figure 66. Von Mises' distribution for a transversal fracture with a Young's modulus of 6000 MPa. Fixator's rod at the top; callus in the middle; bone structure down.

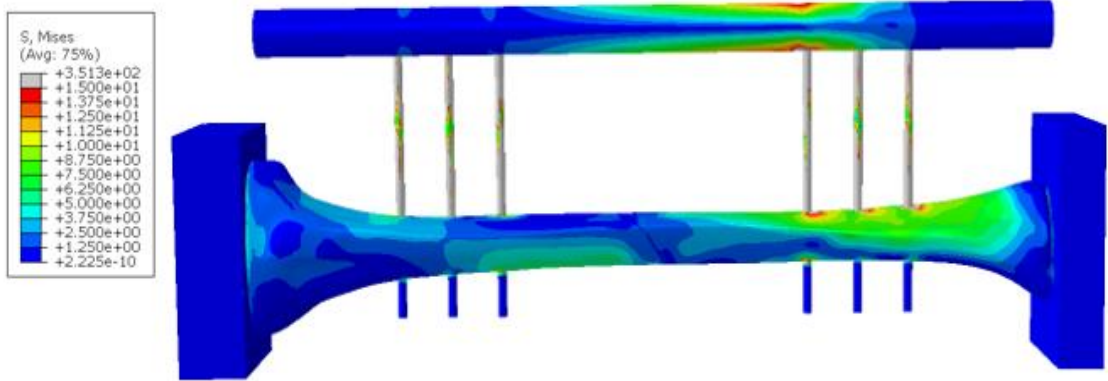


Figure 67. Von Mises' distribution for an oblique fracture with a Young's modulus of 3 MPa.

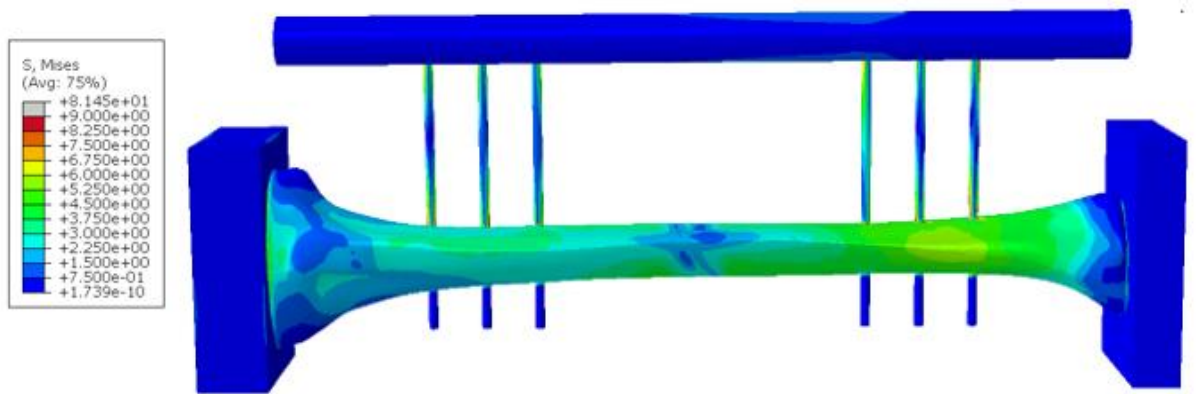


Figure 68. Von Mises' distribution for an oblique fracture with a Young's modulus of 250 MPa.

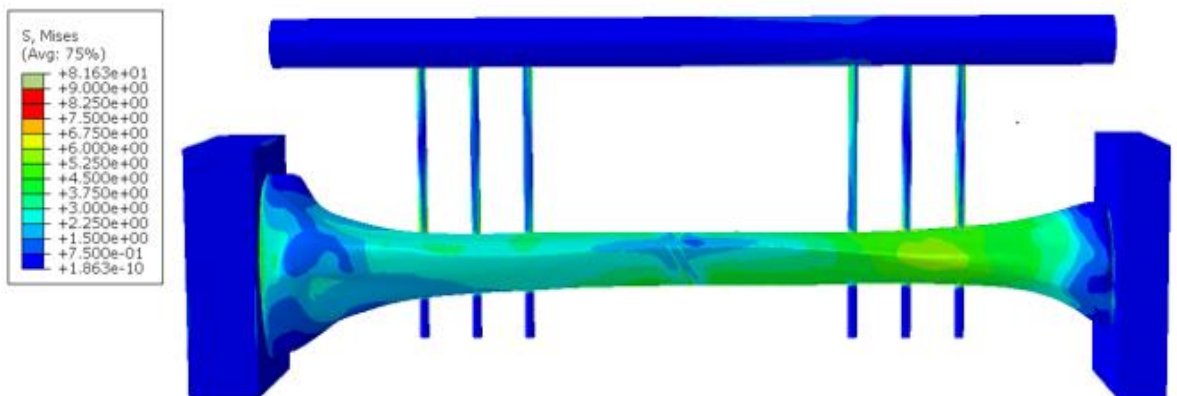


Figure 69. Von Mises' distribution for an oblique fracture with a Young's modulus of 750 MPa.

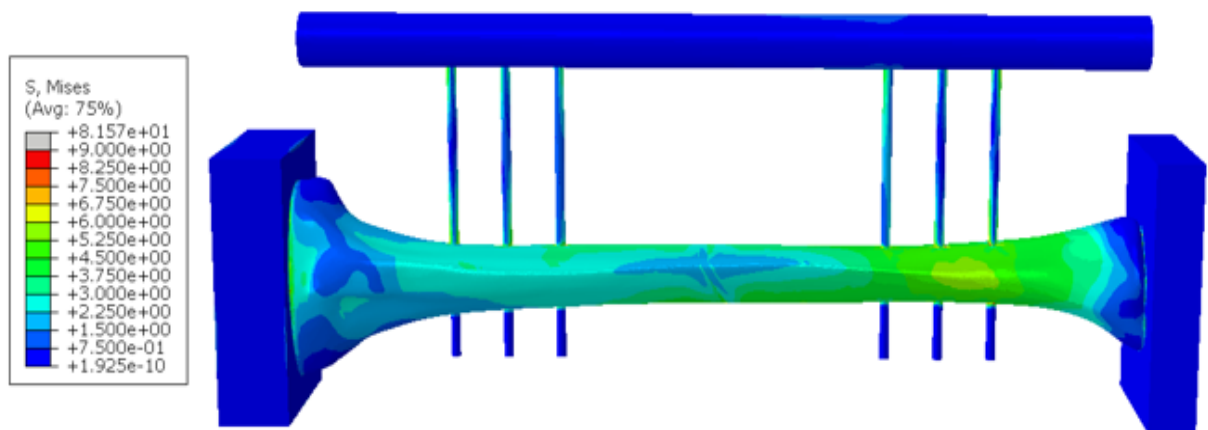


Figure 70. Von Mises' distribution for an oblique fracture with a Young's modulus of 1500 MPa.

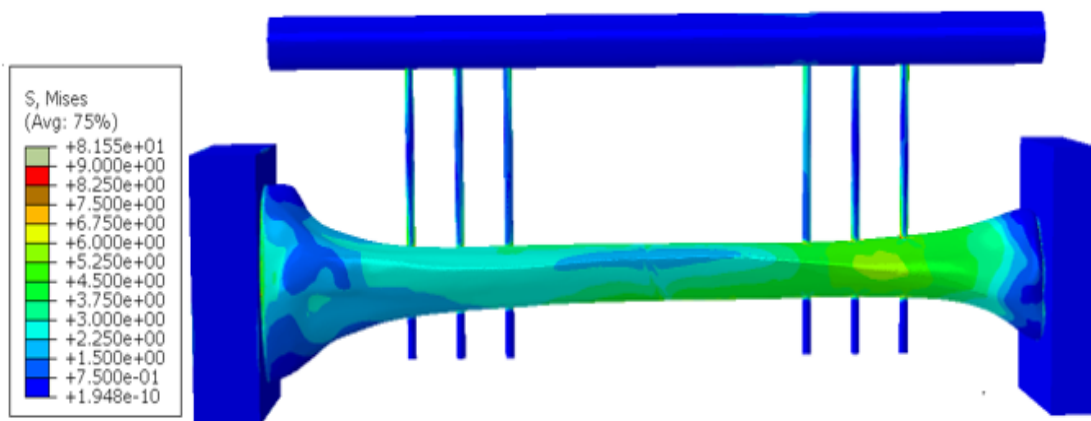


Figure 71. Von Mises' distribution for an oblique fracture with a Young's modulus of 6000 MPa.